Rhenium tricarbonyl complexes of thiazolohydrazinylidene-chroman-2,4-diones derivatives: antibacterial activity and *in vivo* efficacy.

Fatlinda Rahmani,[a] Gozde Demirci,[a] Nikola Plackic, [b] Bettina Tran,[a] Aurelien Crochet,[a] Youri Cortat,[a] Stefan Salentinig,[a] Aleksandar Pavic,*[b] Fabio Zobi*[a]

[a] Department of Chemistry, University of Fribourg, Chemin Du *Musée 9,* 1700, Fribourg, Switzerland

[b] Institute of Molecular Genetics and Genetic Engineering, University of Belgrade, Vojvode Stepe 444a, 11042, Belgrade 152, Serbia

Abstract:

Antimicrobial resistance (AMR) is a major threat to public health, causing serious issues in the successful prevention and treatment of persistent diseases. Transition metal complexes are currently evaluated for the possible development of alternative antimicrobial agents. In our ongoing efforts to identify safe and effective rhenium-based antibiotics, we have prepared a family of compounds bearing derivatives of thiazolohydrazinylidene-chroman-2,4-diones. Two compounds were identified as being active and nontoxic *in vivo* (zebrafish-*S. aureus* ATCC43300 model of infection), efficiently eradicating Methicillin-resistant *Staphylococcus aureus* (MRSA) infection at doses of 500 and 520 ng/mL respectively. *In vitro* studies indicate that, contrary to other known active rhenium complexes, the compounds do not affect peptidoglycan synthesis or compromise the integrity of the cytoplasmic membrane, but rather that bacterial membrane depolarization may play a role in their antibiotic activity.

Keywords: antibacterial, rhenium complexes, MRSA, zebrafish, thiazolohydrazinylidene-chroman-2,4-diones.

1. Introduction

Antibiotic resistance has become a pressing issue in the field of healthcare and medicine. The rise of microorganisms that are resistant to antibiotics poses a significant threat to public health, as it leads to difficulties in treating common infections.[1-3] The overuse and misuse of antibiotics have contributed to the development of resistance in various strains of bacteria, making it imperative to find alternative treatment options and approaches.[4] The World Health Organization has recognized antibiotic resistance as a significant and escalating issue on a global scale. With reports of high levels of resistance emerging from various regions around the world, the urgency to address this issue has become increasingly evident. [5] The problem of antibiotic-resistant species is further highlighted by the World Health Organization's decision to publish a list of germs that it considers the highest priority for the discovery of new antimicrobial drugs [6] particularly against Gram-negative bacteria and members of the *Enterobacteriaceae* family. [7-15] Over the last few years, considerable attention has been paid to the use of inorganic and organometallic compounds for their antibacterial properties. These compounds may offer a practicable alternative to traditional antibiotics and have shown

potential in combating antibiotic-resistant bacteria. [16-21] It's interesting to note that rhenium compounds, which have predominantly been studied for their anti-tumor effects [22-26] have very promising antibacterial activity.[27-35] The landmark study by Metzler-Nolte and Bandow from 2013 marked the beginning of the assessment of the antibacterial potentials of rhenium carbonyl complexes [36]. In their trimetallic complexes, the [(dipicolyl)$Re(CO)_3$] moiety is the crucial component for the antibiotic action of the molecules, as demonstrated by a systematic structure-activity relationship investigation against a variety of harmful bacteria, including methicillin-resistant *S. aureus* MRSA. [37] In the previous investigation from our group, Sovari *et al*. have shed some light on the series-of arylcoumarin of *fac*-[$Re(I)(CO)_3$] complexes for their antimicrobial activities.[38] Sovari *et al*. found that some of the tested complexes exhibited low toxicity *in vivo* and were effective at nanomolar concentrations in the treatment of infections caused by MRSA. The bactericidal effectiveness of the organic 3-arylcoumarin ligands increased by two or three orders of magnitude when coordinated to the *fac*-$[Re(CO)_3]^+$ core. The mechanism of action of the rhenium complexes on bacterial cells was not fully elucidated, but the study indicates that they do not affect the bacterial cell membrane potential. However, it was found that some of the most potent complexes may interact with DNA, suggesting it as a possible target for the compounds. [38] Following Sovari's studies, we decided to focus again on coumarin-type ligands for the rhenium core, and we prepared and investigated the antimicrobial activity of a novel family of Re(I) tricarbonyl compounds with ligands containing coumarin, specifically derivatives of thiazolohydrazinylidene-chroman-2,4-diones. [38-41] The derivatives we describe belong to the class of compounds known as azo compounds. The use of azo compounds is expected to be advantageous, as it expands the possibilities of drug design due to their antibacterial, anti-inflammatory, anthelmintic, antiviral, and anticancer properties.[42] For our molecules we decided to employ, 2-aminothiazole, a typical heterocyclic amine used in the synthesis of a wide range of compounds, including sulphur-containing medicines, biocides, fungicides, [43-45] and 4-hydroxycoumarin due to its dominance in natural product chemistry, with a variety of pharmacological effects, and good optical qualities. [46-51] In this contribution we highlight the synthesis of the family of complexes, their antibiotic effectiveness both *in vitro* and *in vivo* for the least toxic compounds and attempts to better understand their mode of action by analyzing their effects on the bacterial membrane and peptidoglycan biosynthesis.

2. Results and discussion

2.1 Synthesis and characterization of ligands and complexes

The synthesis of the thiazolohydrazinylidene-chroman-2,4-diones ligands involves the diazotization of 2-aminothiazole derivatives and their subsequent coupling to 4-hydroxycumarin (Scheme 1). Ligands **L1**, **L2**, **L4** and **L6** were prepared following a published procedure [39], while ligands **L3** and **L5** were prepared according to a specified procedure, adapted for our needs. [40, 41] These ligands were then used in the synthesis of *fac*-[$Re(CO)_3$(N⁀N)Br] complexes **1-6**, as illustrated in Scheme 1. The pentacarbonyl precursor [$Re(CO)_5Br$] was synthesized by the reaction of dirhenium decacarbonyl [$Re_2(CO)_{10}$] with bromine [52] and then complexed with **L1-L6**. Specifically, the required *fac*-

[Re(CO)$_3$(N⁀N)Br] complexes were synthesized in a one-pot reaction by the decarbonylation of [Re(CO)$_5$Br] in the presence of the bidentate ligands in dry toluene, according to the published procedure.[53] The one-pot reaction method not only facilitated the synthesis and purification process but also resulted in high yields of the desired complexes. Under these conditions, complexes **1-6** spontaneously precipitate from the reaction mixture and their isolation was carried out via vacuum filtration. Additionally, yields of complexes **1-6** were as high as 92%.

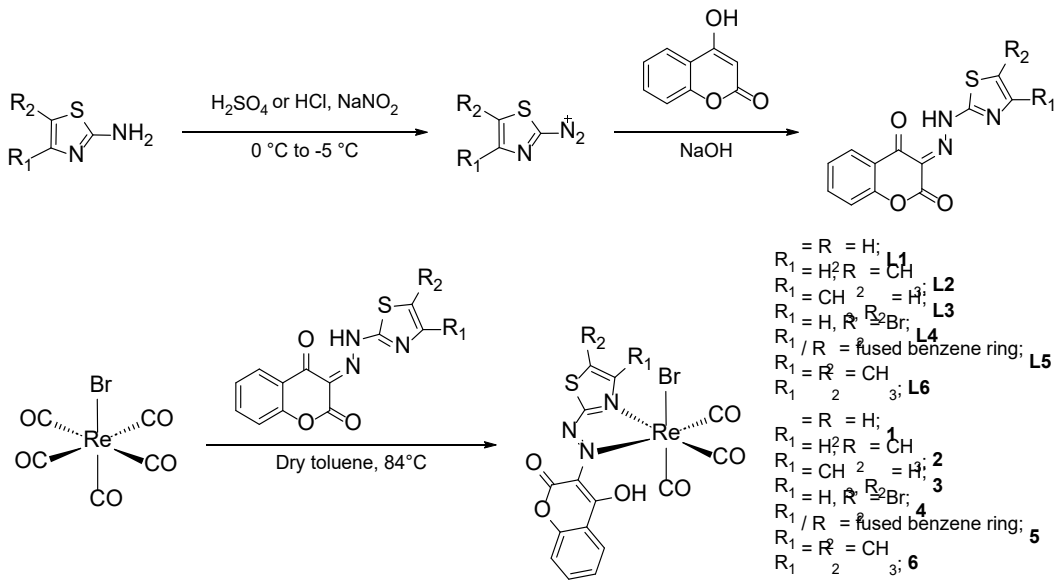

Scheme 1. General synthetic procedures and chemical structures of ligands **L1-L6** and bromo rhenium complexes **1-6**.

Ligands **L1-L6** might theoretically take five distinct tautomeric forms [40] (Scheme 2). The diketo form "a" (Scheme 2) prevails as the most stable tautomeric conformer for compounds **L1-L4** and **L6** according to previously reported gaseous phase calculations [54] while the diazenyl form "c" of compound **L5** was predicted as the most stable tautomer. [41] Taking into account the nature of the ligands and heteroatoms present in their structure, from the TD-DFT calculations, the most stable form of the corresponding *fac*-[Re(CO)$_3$(N⁀N)Br] complexes, was predicted as the N=N bound form A (Scheme 2). However, when the complexes are exposed to a coordinating solvent (H$_2$O, DMSO, MeOH, CH$_3$CN), structure B (Scheme 2**,** S* = coordinating solvent) prevails. Typically, coordinating solvents have the ability to substitute Br, leading to a positively charged complex of formula *fac*-[Re(CO)$_3$(N⁀N)S*]$^{+\cdot}$ We found that, under these conditions, the coumarin OH group is easily deprotonated and coordinates to Re, stabilizing at the same time the charge of the complex.

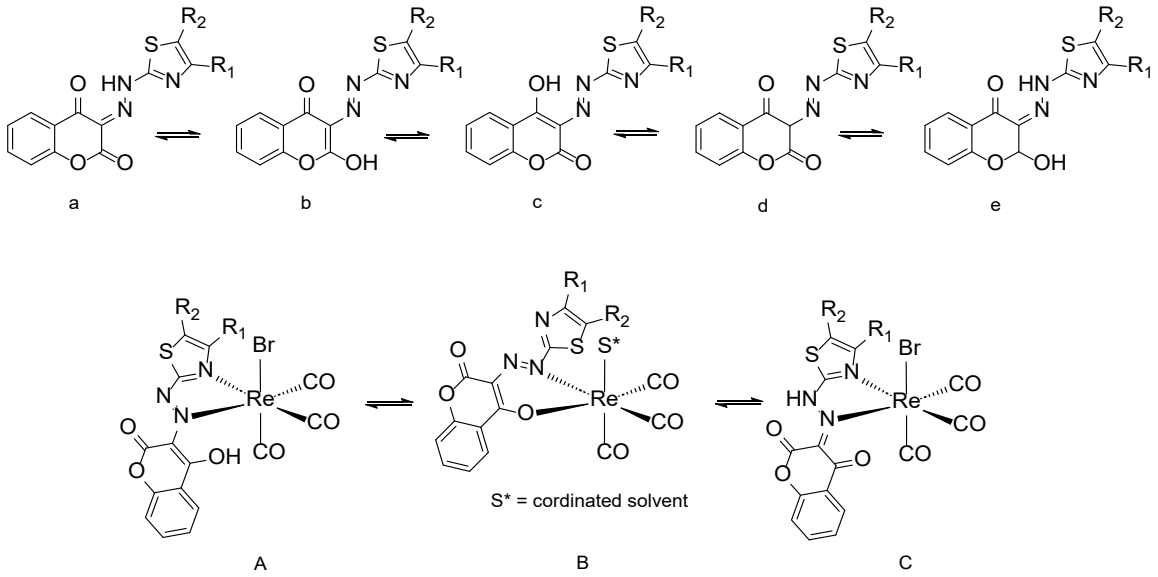

Scheme 2. Possible tautomeric forms of ligands **L1**-**L6** (top) and of complexes **1**-**6**.

The ^{1}H NMR spectra of **1-6** in coordinating solvents revealed a plethora of signals (Figure 1) due to the equilibrium established amongst the tautomeric form of the ligand bound to Re atom (structures A, B and C, Scheme 2). It is noteworthy to mention that ^{1}H NMR spectroscopy (in dry CD_2Cl_2) reveals that it is the form C of the complex (Scheme 2) that it is obtained as a reaction product. In terms of characterization and photophysical properties, complexes were fully characterized by ^{1}H NMR, ^{13}C NMR, IR spectroscopy, and UV-Vis spectroscopy (ESI). As expected, infrared spectra of rhenium complexes **1-6** showed two characteristic bands corresponding to the υ(CO) symmetric and asymmetric stretching modes around 2022 and 1916 cm^{-1}. The UV-Vis spectra of complexes **1-6** are all very similar. They have an intense absorption band around 560nm, with a lower absorption band at about 360nm and a shoulder at 270-290 nm. In addition, none of the complexes exhibits fluorescence characteristics.

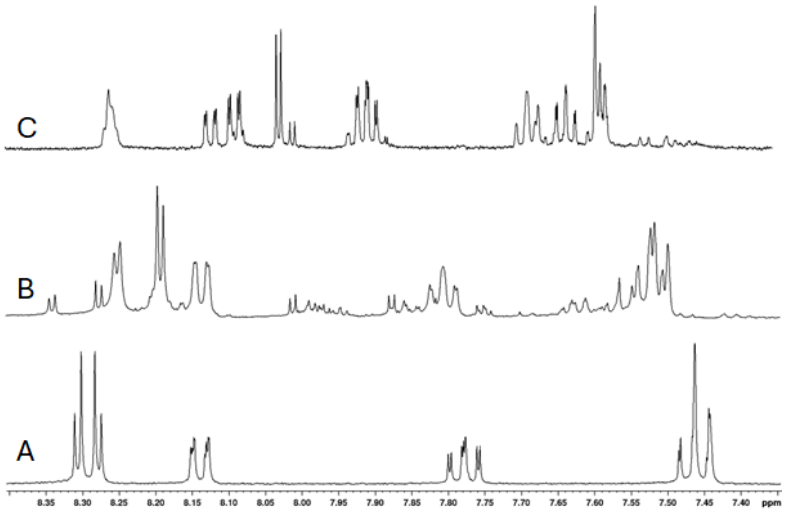

Figure 1. ^{1}H NMR spectra of complex **1** in CD_2Cl_2, DMSO-d_6 and CD_3CN (A, B and C respectively) with a focus on the aromatic region.

Having prepared complexes **1-6**, we decided to further expand the library of compounds by substituting the coordinated Br by neutral monodentate ligand such as pyridine (py). The reason for this choice is based on previous results published by Sovari *et al.* study [34], who demonstrated that cationic, mostly py, tricarbonyl complexes show better activity and lower *in vivo* toxicity than similar neutral bromide species. To this end, we set out to synthesize *fac*-$[Re(CO)_3(N^{\frown}N)\#L\#]^+$, where L# = pyridine or other monodentate ligands and $(N^{\frown}N)\#$ = structure A (Scheme 2) of ligands **L1-L6**. However, despite our efforts, the reaction of $[Re(CO)_5Br]$ in the presence of the bidentate ligands **L1-L6** and L# always resulted in *fac*-$[Re(CO)_3(O^{\frown}N)\#L\#]$ complexes (**7-16**, Scheme 3) where $(O^{\frown}N)\#$ = the diazenyl structure B (Scheme 2) of ligands **L1-L6**. The deprotonation of the coumarin OH group and its binding to Re results in the formation of neutral, rather than the desired cationic, complexes.

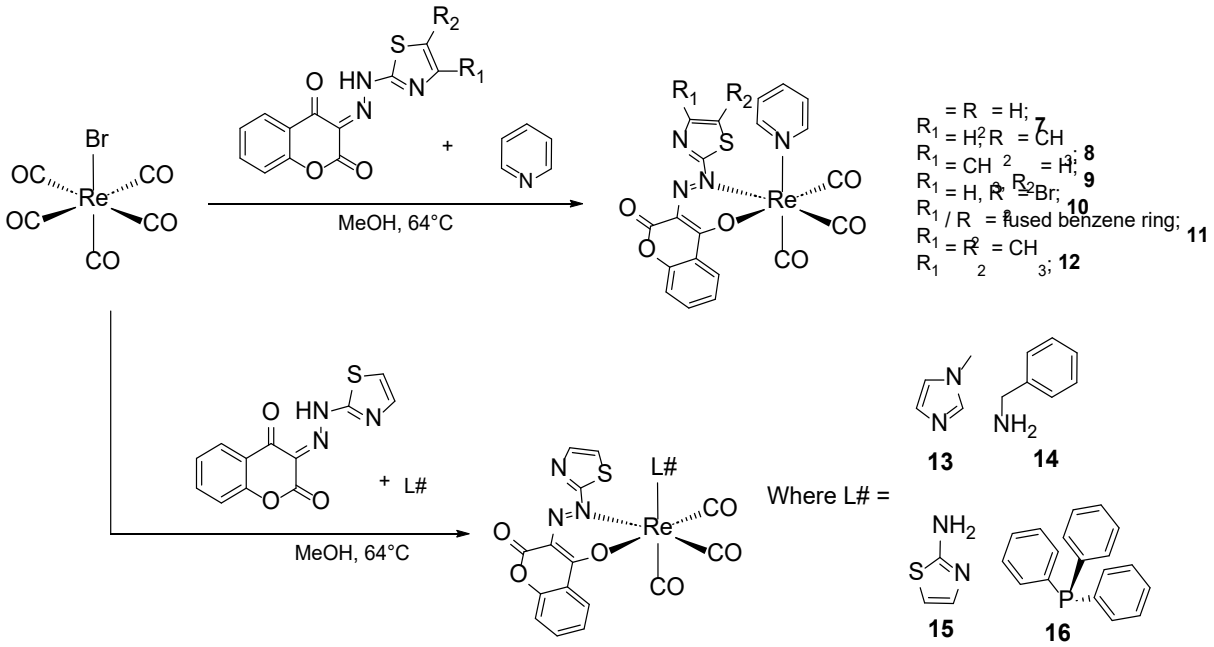

Scheme 3. General synthetic procedures and chemical structures of complexes **7-16**.

Nevertheless, using a mixture of ethyl acetate and hexane as an eluent, the purification and isolation of the rhenium complexes in the crude mixtures was successfully carried out by column chromatography. After the column chromatography process, the isolated fractions (R*f* values are displayed in ESI, Figure S48) containing the complexes were subjected to lyophilization, resulting in the formation of dry powders, suitable for further characterization and analysis. Contrary to **1-6**, compounds **7-16** show clean ^{1}H NMR and ^{13}C NMR spectra in coordinating solvents, indicating that the structures are the thermodynamically stable tautomeric forms, and that the species do not exchange L# for solvents. Similarly to **1-6**, compounds **7-16** show characteristic υ(CO) symmetric and asymmetric stretching in their IR spectra and do not exhibit fluorescent properties.

2.2 X-ray crystallography

In this study we succesfully managed to crystallize several of the molecules described above. Ligands **L1**, **L2**, **L4** and **L6** were crystallized using a variety of methods and their structures are given in ESI (Figure S47). They show similar structural parameters as **L3**, previously disclosed.[40] In order to fully understand how coordinating and non-coordinating solvents affected the structure of the complexes, many attempts were carried out to crystallize the complexes using different types of solvents. It is enthralling to notice how the type of solvent may determine the coordination mode of **L1**-**L6** and the resulting structure of *fac*-[$Re(CO)_3(N^{\frown}N)Br$] type complexes. For compound **1** two distinct crystal structures were determined. The first crystal was obtained by dissolving compound **1** in DMSO and then layering it with H_2O, at R.T. The results indicate that Br was substituted by H_2O, while the coumarin OH group deprotonated and formed a new bond to Re. The second crystal was grown by dissolving compound **1** in dry CH_2Cl_2 and then layering it with dry pentane, at R.T. In this case, there is no change in the structure of *fac*-[$Re(CO)_3(N^{\frown}N)Br$] (A, Scheme 2). Figure 2 depicts the crystal structure of these tautomers.

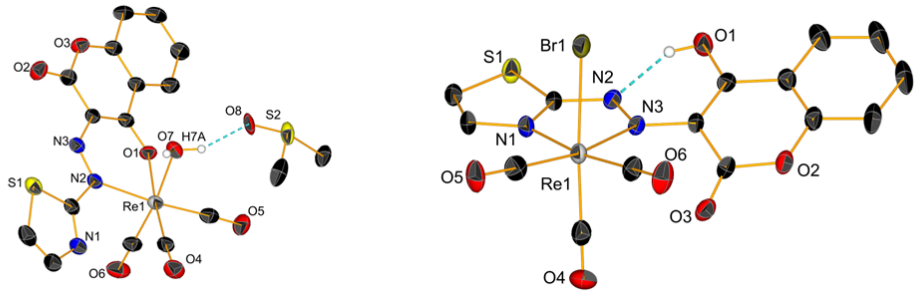

Figure 2. Crystal structures of complex **1**, in two distinct tautomer forms observed respectively in coordinating (left) and non-coordinating solvents. Thermal ellipsoids are at 30% probability. Hydrogen atoms are omitted for clarity.

Compounds **2** and **6** were crystalized in dry CH_2Cl_2 and dry pentane. The crystallization of compound **5** was carried out via slow evaporation of a MeOH solution. MeOH behaves similarly to H_2O in that Br was substituted while the coumarin OH group deprotonated and coordinated to Re. With the exception of compound **1** in DMSO:H_2O, which crystallized in the triclinic lattice in P-1 space group, all of the other complexes crystallized in a monoclinic lattice in the $P2_1/c$ space group. Figure 3, displays the crystal structures of **2**, **5**, and **6**.

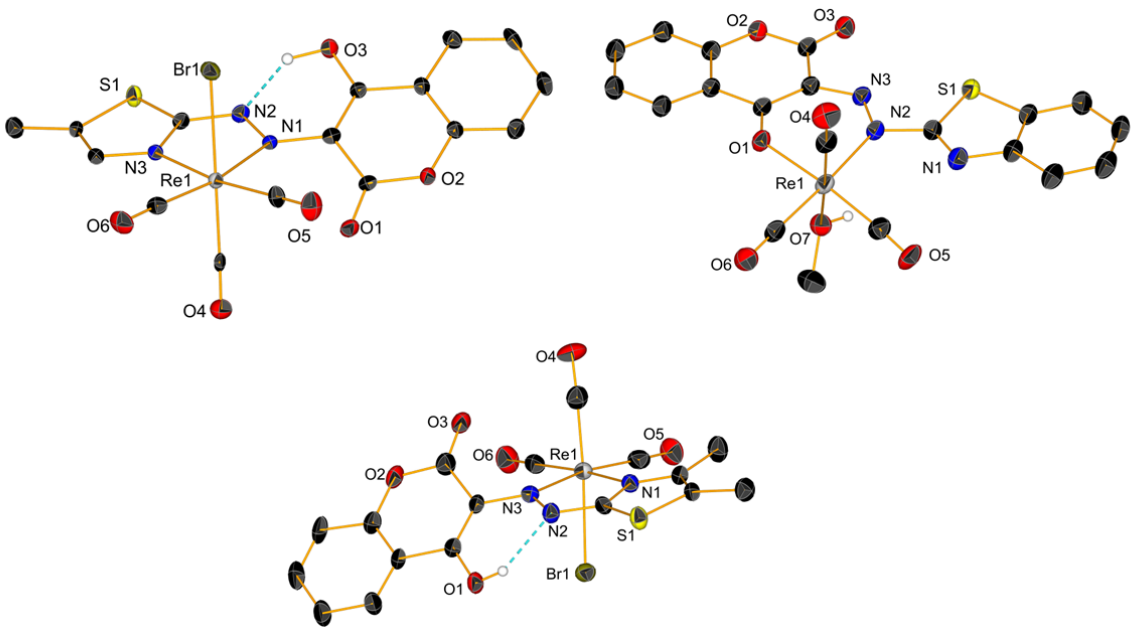

Figure 3. Crystal structures of complexes **2**, **5** (top), and **6**. Thermal ellipsoids are at 30% probability. Hydrogen atoms are omitted for clarity.

The crystal structures of compounds **7**, **8**, **9** and **12** are shown in Figure 4. Compound **7** crystalized by layering CH_2Cl_2 and pentane, in the triclinic crystals system, P-1 space group. Compound **8, 9** and **12** (all characterized by a coordinated py) crystalized by layering diethyl ether on a CH_3CN solution of the molecules. Complexes **8** and **9** crystallized in triclinic crystal system, P-1 space group, while compound **12** in monoclinic crystals system, $P2_1/c$ space group. Finally, single crystals of **13**, **15** and **16** suitable for X-ray diffraction analysis (Figure 5) were obtained by slow evaporation of either MeOH or CH_3CN solutions of the compounds.

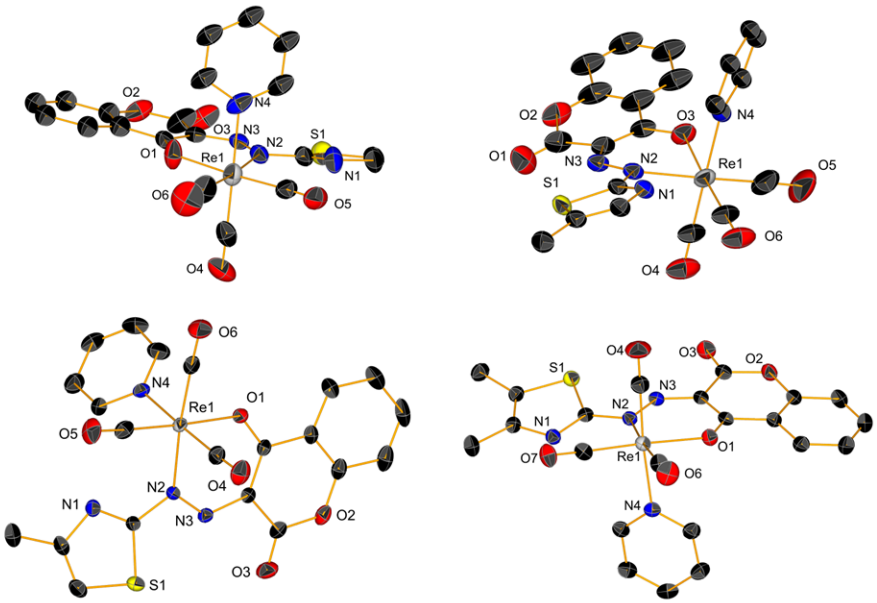

Figure 4. The crystal structure of complexes **7**, **8** (top), **9** and **12**. Thermal ellipsoids are at 30% probability. Hydrogen atoms are omitted for clarity.

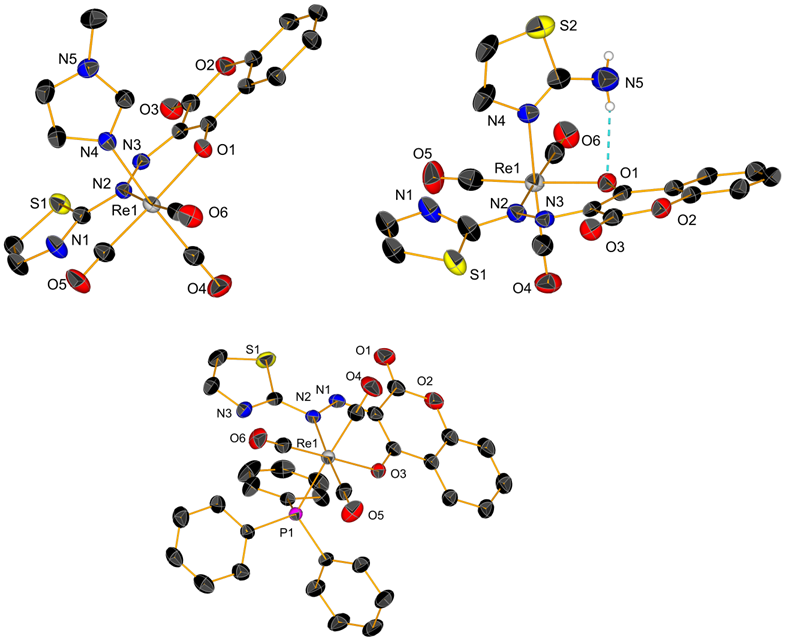

Figure 5. the crystal structure of complexes **13**, **15** and **16**. Thermal ellipsoids are at 30% probability. Hydrogen atoms are omitted for clarity.

2.3 In vitro cytotoxicity and antimicrobial activity of molecules.

Essential to this research is the study of the biological properties of each complex to determine their potential antimicrobial properties and toxicity. As a first step we then conducted *in vitro* assays to determine the cytotoxicity and the minimum inhibitory concentration of the compounds, followed by *in vivo* toxicity studies in zebrafish to evaluate their effects on living organisms. *In vitro* cytotoxicity studies on mouse fibroblast L929 cells indicated that most of the tested complexes do not show significant toxicity at concentrations below 10 μM (ESI, Figures S549-S51). The antimicrobial activity of the ligands and complexes was then evaluated against two *S. aureus* strains and two *Candida* strains, namely *C. albicans* and *C. auris 7*. Table 1 and 2 give the collected data of **L1**-**L6** and **1**-**15** respectively. While all ligands were effective against *S. aureus* strains, but ineffective against the fungi, they showed similar *in vivo* toxicity and consequently a very low therapeutic index (Ti). Coordination of the ligands to the *fac*-$[Re(CO)_3]^+$ core did not generally improve the efficacy of the complexes with the exception of **2** and **6**. These two compounds showed a good MIC value against *S. aureus* strains (3.13 and 1.6 μM respectively), but more importantly low toxicity *in vivo* (LC50 values >50 μM for **2** and ca. 35 μM for **6**) and very good Ti's (>16). To our surprise, complexes **7**-**15** were completely inactive against the pathogens, suggesting perhaps that a weakly coordinated monodentate ligand may be required (but not sufficient) for the antibiotic action of this family of complexes. Finally, none of the molecules tested showed any activity against *Candida* strains.

Table 1. Minimum inhibitory concentration (MIC, μM), LC50 and therapeutic index (Ti) of ligands **L1-L6** against MRSA, MSSA and fungal strains.

Compound	LC50	*C. albicans*	*C. auris 7*	MRSA	MSSA	Ti
L1	<2.5	>50	>50	12.5	12.5	0.23
L2	3.5	>50	>50	12.5	12.5	0.28
L3	<2.5	>50	>50	12.5	12.5	0.23
L4	<2.5	>50	>50	12.5	6.25	0.2
L5	3.5	>50	>50	6.25	<1.6	0.56
L6	<2.5	>50	>50	<1.6	3.13	1.56

Table 2. Minimum inhibitory concentration (MIC, μM), LC50 and therapeutic index (Ti) of Complexes **1-16** against MRSA, MSSA and fungal strains. *

Compound	LC50	*C. albicans*	*C. auris 7*	MRSA	MSSA	Ti
1	3.5	>50	>50	3.13	3.13	1.1
2	>50	>50	>50	3.13	3.13	>16
3	3.5	>50	>50	12.5	25	<1
4	3.5	>50	>50	1.6	1.6	2.2
5	7.1	>50	>50	1.6	1.6	4.4
6	34.7	>50	>50	1.6	1.6	21.7
7-15	n.d.	>50	>50	>50	>50	n.d.

* Complex **16** was not tested due to some impurities that could not be removed by HPLC or column chromatography.

*2.4 In vivo effects of **2** and **6** against MRSA infection.*

Having established the antimicrobial potency of the complexes, we decided to investigate the *in vivo* efficacy of **2** and **6** against MRSA using the zebrafish-*S. aureus* ATCC43300 model of infection. To this end, systemic infection of zebrafish embryos was accomplished by injecting 1500–1600 fluorescently labelled bacterial cells into their bloodstream 34-hours post fertilization (hpf). Infected embryos were then exposed to $^{1}/_{8}$ × to ½ × MIC doses of **2** and **6** and inspected, over a period of 4 days post infection (dpi), for survival and bacterial cell occurrence (fluorescence) as measures of their antibacterial efficacy. We found that **2** and **6** successfully rescued zebrafish embryos from lethal MRSA infection during a 4-day treatment, with the protective effect being evident already at 24–48 hours post injection (hpi) at ¼ and ½ × MIC dose respectively ($P < 0.001$, log-rank test, Figure 6A). While untreated embryos developed large pericardial edema by 48 hpi with strong red fluorescence originating from labelled *S. aureus*, and progressively died by 4 dpi (mortality rate of 60%), fish treated at ¼ × MIC of **2** and ½ × MIC **6** had markedly reduced bacterial load (based on fluorescence signal, Figure 6B), and all survived by 4 dpi. Based on the survival rate of infected embryos by 4 dpi, **2** and **6** increased the infected embryos survival rate to 100% at the dose of ½ × MIC, compared to that in untreated group. Moreover, at 48 h post treatment, at 0.8 μM dose, no detectable fluorescence of labelled *S. aureus* cells was observed within the body of the infected animals, suggesting effective MRSA infection eradication (Figure 6A). Less effective were the complexes at 0.4 μM doses, with embryos' survival reduced to 80 and 50% respectively for **2** and **6** at 4 dpi. Taken together, the data obtained in this infection assay indicate that **2** and **6** are efficient and safe agents against MRSA infection *in vivo* at doses of 500 and 520 ng/mL respectively.

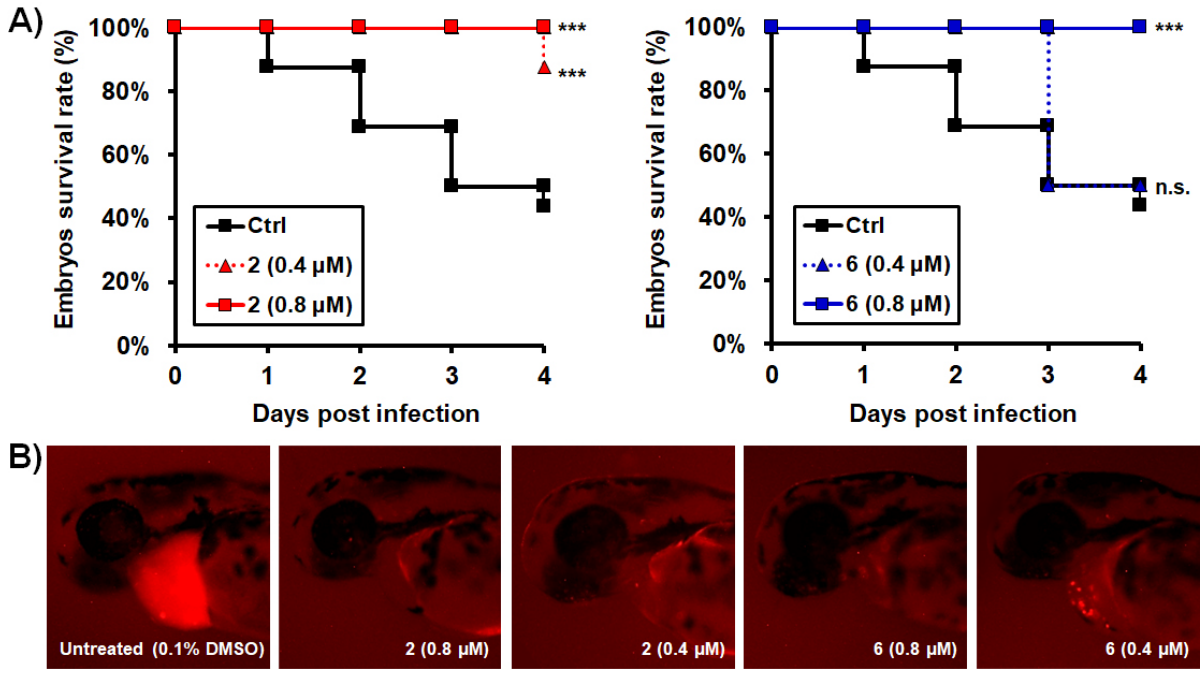

Figure 6. Complexes **2** and **6** successfully rescued zebrafish embryos from the lethal MRSA-infection. Wild (AB) zebrafish embryos were infected with 1500–1600 fluorescently labelled

cells of *S. aureus* ATCC43300 (MRSA) into the circulation valley and treated with different doses of the tested complexes for 4 days. The antibacterial efficacy of the applied complexes was assessed by monitoring the survival of MRSA-infected embryos (Kaplan-Meier survival curves, A) and fluorescence of bacterial cells burden (red fluorescence in the panel B) during a course of 4-days treatment (n = 20). Signs of multiplied infection in untreated embryos were visible already at 24 h after bacterial cells injection, while infection burden was markedly suppressed upon application of **2** and **6**, especially at 0.8 μM doses of complexes. Significance in the survival rates between treated and untreated embryos is indicated with asterisks (∗P < 0.05; ∗∗P < 0.01; ∗∗∗P < 0.001).

2.4 Mechanism of action studies

Only limited data are available on the mechanism of action of antibiotic rhenium complexes, but effective compounds are reported to either inhibit membrane-associated stages of peptidoglycan (PG) synthesis [35] or affect the bacterial membrane. [36] We also decided to investigate the impact of **2** and **6** on the PG biosynthesis and the bacterial cytoplasmic membrane. Disruption of the PG synthesis process can be monitored with the fluorescent amino acid derivative 7-hydroxycoumarincarbonylamino-d-alanine (HADA). In microbiology HADA is widely used in this context for different bacteria [55], including *S. aureus*.[56] The microorganisms incorporate HADA during the extra-cytoplasmic stage of PG synthesis through activity of transpeptidases [57], and the use of HADA allows monitoring sites of emerging PG or its spatial distribution. Exposure of *S. aureus* cells to **2** and **6** at 2× their MIC value did not significantly affect HADA incorporation in the PG of MRSA, while, within experimental error, the relative fluorescence intensity of the amino acid derivative only slightly decreased in treated cells at 4×MIC of **2** and **6** (Figure 7). Next, we decided to determine the activity of the complexes in a checkboard assay with vancomycin. The drug is an important antibiotic recommended in several countries for the treatment of MRSA, [58-61] and it acts by inhibiting the second stage of cell wall biosynthesis. The results of our experiments indicate that fractional inhibitory concentration index of the vancomycin/rhenium complexes chequerboard assays is between 0.75 and 1, indicating no interaction (i.e. an indifferent effect) between the drugs, further suggesting that **2** and **6** may not act on the PG biosynthesis. Finally, we investigated the binding affinity (docking scores) of **6** in its two tautomeric forms with all MRSA proteins involved in peptidoglycan biosynthesis (detailed data are provided in ESI, Figure S52). Of the enzymes involved, the penicillin-binding proteins (PBPs) were of particular interest to us since they are the transpeptidases that perform the crosslinking reaction in the synthesis of the peptidoglycan backbone which would involve incorporation of HADA. [62-65] Indeed, complex **6** showed amongst the lowest binding affinity with PBPs (ESI, Figure S52). Taken together, the results imply that **2** and **6** have little effect on the PG biosynthesis, and inhibition of the same is unlikely to play a role in the mechanism of action of the molecules.

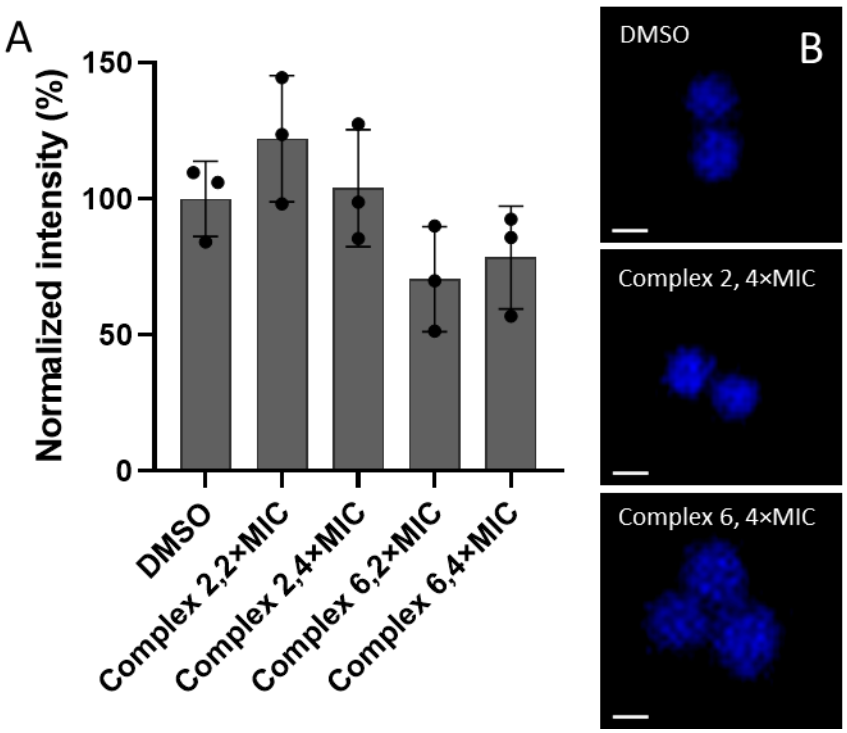

Figure 7. HADA incorporation into *S. aureus* peptidoglycan biosynthesis. A. Relative HADA fluorescence intensities quantified from ≥200 cells per experiment from three independent biological replicates. B. HADA labelled *S. aureus* ATCC25923 cells after a 10min exposure to **2** and **6** at 4×MIC concentration. DMSO (0.5%) was used as the negative control. Microscopic settings were kept constants for all micrographs. Scale bar, 5μm.

Next, we investigated the effect of **2** and **6** on the cytoplasmic membrane of MRSA. First, we evaluated changes in the membrane potential of the bacterium. To this end we used the 3,3′-diethyloxacarbocyanine iodide [$DiOC_2(3)$] fluorescent dye. [$DiOC_2(3)$] exhibits a green fluorescence in cells with a normal or depolarized membrane potential. However, when the membrane potential becomes hyperpolarized (more negative inside the cell), [$DiOC_2(3)$] aggregates and exhibits a red-shifted fluorescence emission. The ratio of red to green fluorescence is often calculated as an indicator of membrane potential, allowing to monitor the dynamic changes in bacterial membrane potential in response to different drugs. Both **2** and **6** significantly reduced membrane potential at 1× MIC, with the effect being more pronounced as a function of the increasing concentration of the complexes (Figure 8). Although, the effect of the compounds was not as severe as the one induced by protonophore carbonyl cyanide m-chlorophenylhydrazone (CCCP), it is possible that bacterial membrane depolarization may play a role in in the antibiotic effect of **2** and **6**.

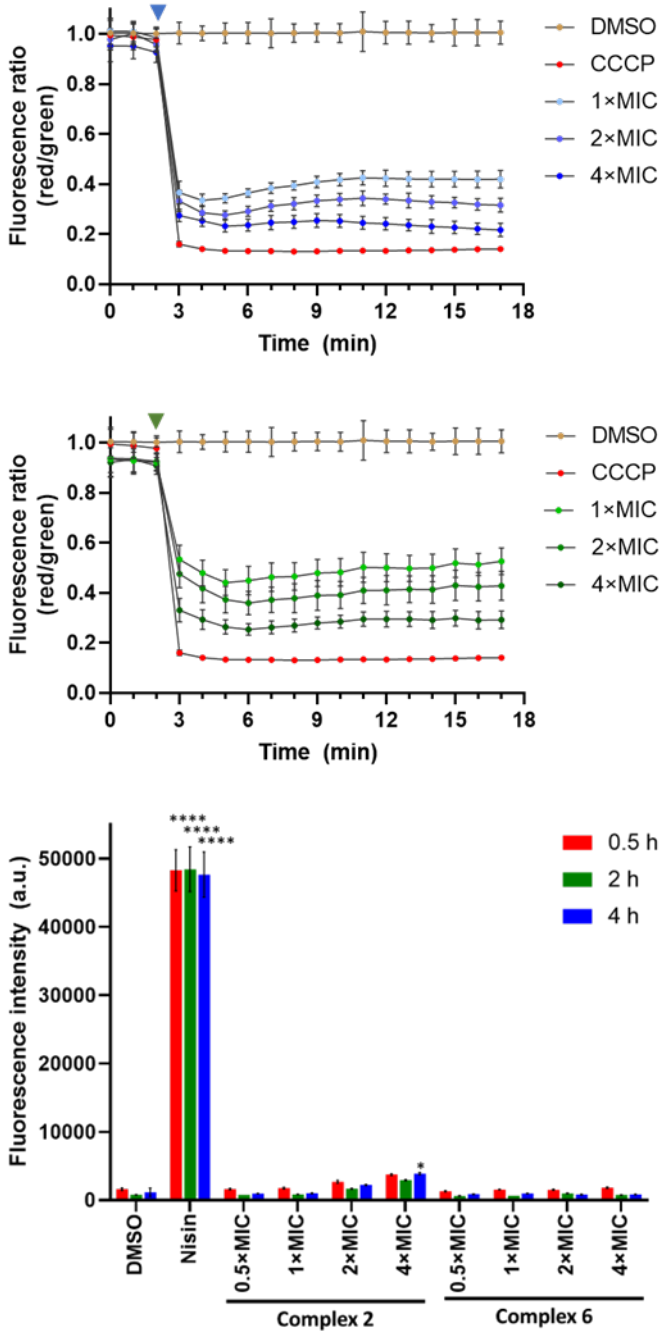

Figure 8. Time-dependent effect of **2** (top) and **6** (middle) on the membrane potential of *S. aureus* ATCC25923 cells. Membrane potential was measured as a function of the red to green fluorescence ratio of [$DiOC_2(3)$]. Protonophore CCCP (25 µM, 2×MIC) was used as a positive control and DMSO as a negative control. Bottom, PI fluorescent intensity of *S. aureus* cells treated with DMSO (1%), Nisin (100 µg/mL) and 4 different concentrations of complexes **2** and **6** at three different time points. Statistical analysis was performed against DMSO treated control cells. Statistical significance: (*) $p < 0.0332$, (**) $p < 0.021$, (***) $p < 0.0002$, (****) $p < 0.0001$.

We then examined the integrity of the cytoplasmic membrane by exposing MSSA cells to **2** and **6** and to the non-permeant, positively charged propidium iodide (PI) dye in a concentration and time-dependent assay (Figure 8). PI is impermeable to viable bacteria with intact membranes but can penetrate cells with compromised membranes. Once inside the cell, PI intercalates into DNA bases forming a strong red-emitting fluorescent complex. [66] Contrary to the positive control nisin, neither **2** or **6** allowed penetration of PI in MSSA cells, clearly excluding the possibility that the mode of action of the compounds is related to disruption of membrane impermeability or its barrier function.

Finally, we performed small-angle X-ray scattering (SAXS) analysis and analyzed *in silico* the interaction of **2** and **6** with a semi-flexible POPE:POPG membrane model. SAXS is a powerful technique used to study the structure of biological membranes at the nanometer scale. It can provide detailed information about the size, shape, and structural changes of membranes. The SAXS curve of the untreated Gram positive (g+) vesicles (POPE:POPG at a weight ratio of 1:3) before the addition of the complexes are characteristic of oligo-lamellar vesicles. In the low-q values ($q < 0.3$ nm^{-1}) the scattering decays approximately as $q^{-2.6}$. The overall dimensions of the vesicles are beyond the accessible q-range of our set-up, which is 30 nm, calculated with $D_{max} = PI/q$. A broad correlation peak can be observed in the q-range of 0.1-3 nm^{-1}, with further undulations at higher q-values arise from the electron density differences in the thickness region of the vesicle bilayer. This excess electron density, relative to the buffer, is lower for alkyl chains and higher for the phosphate head-groups with their associated counter ions. The additional shoulder around $q = 0.4$ nm^{-1} may arise from the inter-bilayer scattering in the oligo-lamellar vesicles (Figure 9A).

Upon addition of complexes **2** and **6**, the signal-to-noise ratio in the SAXS curves increases significantly in the q range below 0.5 nm^{-1} (Figure 9A). The first minimum in the SAXS curve also shifts from q around 0.3 nm^{-1} to around 0.6 nm^{-1}. This demonstrates the interaction of the complexes with the vesicle bilayer. The accumulation of the rhenium complexes in or at the negatively charged vesicle bilayer increases the excess electron density, which increases the scattering signal. The modified electrostatic interactions among the charged headgroups can modify the curvature of the bilayer. The electrostatic repulsions between the lamellar layers in the oligolamellar vesicles is also influenced, as indicated by the change in power-law scattering. This interaction appears more prominent for compound **6**. The low-q power law scattering exponent decreases from -2.6 for the g+ vesicles to around -2.8 for compound **2** and -3.6 for compound **6**. As the power-law exponent increases with the number of layers in oligo- and multi-lamellar vesicles, this may result from an increase in the number of layers and/or ordering as a result of modified bilayer interactions upon adsorption of compound **6**.

The results of the theoretical calculations (Figure 9B), confirm the experimental SAXS results in that in the lowest energy poses, **6** appears to more strongly interact with 1:2 POPE:POPG membrane model as compared to **2**. This latter compound does not deeply penetrate in the lipid layer, but rather "hovers" above or weakly interacts with it, while **6** more prominently interacts with the membrane model (Figure 9B), confirming that the interaction of the complexes with the vesicle bilayer is predominantly electrostatic in nature as indicated by SAXS data. Finally, the calculations indicate that both compounds cause a structural rearrangement of the flexible

lipids as compared to the initial 1:2 POPE:POPG membrane model. This rearrangement may relate to the observed modification of the electrostatic repulsions between the vesicle bilayer resulting in the decreased distance between the lamellar layers in the oligolamellar vesicles observed in the SAXS experiment.

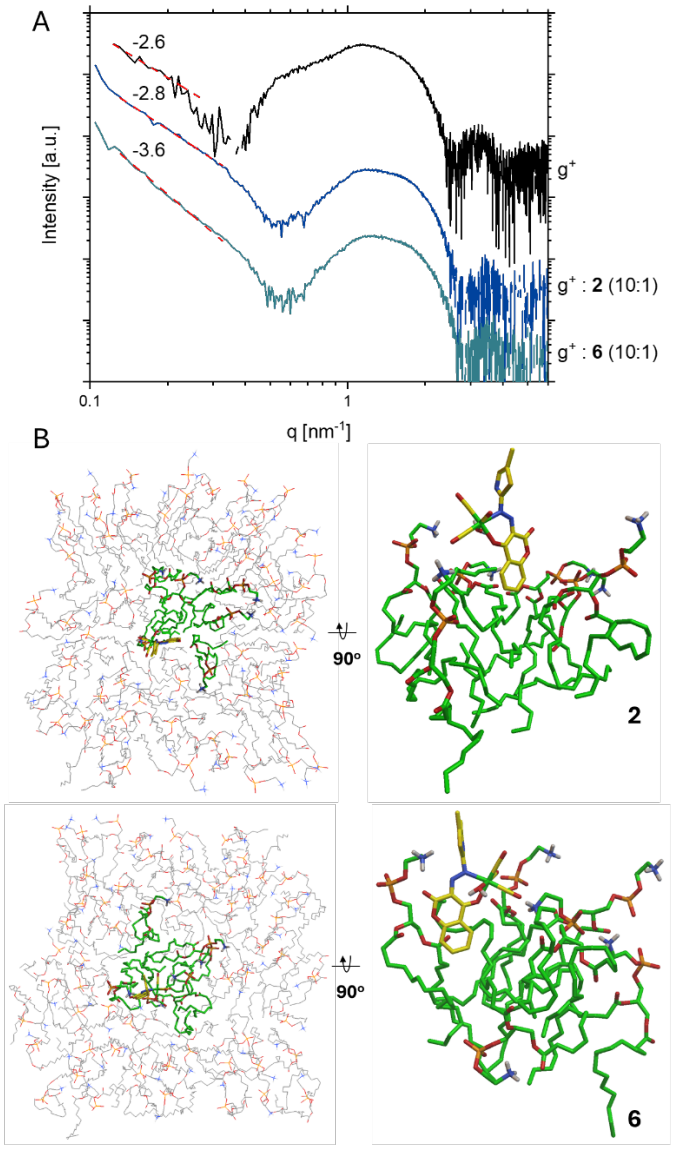

Figure 9. A. SAXS pattern of g^+ vesicles (POPE: POPG at a weight ratio of 1:3) before (black curve), and after addition of complex **2** (blue curve) and complex **6** (green curve). B. Top and detail side views of lowest-energy conformation of complexes **2** and **6** in the semi-flexible 1:2 POPE:POPG membrane model (flexible lipids are shown in green).

3. Conclusion

We have reported in this study the synthesis, characterization, antibacterial activity and *in vivo* efficacy of a library of molecules, including 16 rhenium complexes bearing derivatives of thiazolohydrazinylidene-chroman-2,4-diones as ligands. Whereas the ligands were active against the bacteria, they showed toxicity *in vivo* if administered alone, but from the library of the metal complexes we identified two compounds (**2** and **6**) as being active and nontoxic *in vivo* (zebrafish-*S. aureus* ATCC43300 model of infection), efficiently eradicating MRSA infection at doses of ca. 500 ng/mL and with a therapeutic index >16. Compared to the control group, at their active doses, **2** and **6** increased the infected zebrafish survival rate to 100%, preventing the same from developing large pericardial edema. *In vitro* studies, indicated that, contrary to other known active Re complexes, **2** and **6** do not affect peptidoglycan synthesis or compromise the integrity of the cytoplasmic membrane of MSSA, but rather that bacterial membrane depolarization may play a role in the antibiotic effect of the compounds. These results are markedly different from similar coumarin based complexes [38] underscoring at the same time the difficulty in predicting the mode of action of the compounds, but also the great development prospective that these class of molecules holds. Overall, our study further highlights a real antibiotic potential of rhenium tricarbonyl species within a growing field of research ultimately aimed at answering the WHO call for a comprehensive overview of non-traditional antibacterial medicines to address the growing threat that antibiotic resistance poses. Future works from our groups will focus on expanding the library of Re-based complexes to identify new unique active structures and on the elucidation of their mechanism of action in our continued development and discovery of new and highly potent antimicrobial agents.

4. Experimental Section

Materials and Methods

4.1. Reagents and chemicals

All reagents were purchased from standard sources. Acros Organics provided the 2-aminothiazole, 2-aminobenzothiazole, pyridine and benzylamine, 1-methylimidazole and [$Re(CO)_{10}$] were purchased from Sigma-Aldrich, 4-methyl-2-aminothiazole, 5-methyl-2-aminothiazole, 5-bromo-2-aminothiazole monohydrobromide and clotrimazole were purchased by Fluorochem 4,5-dimethyl-2-aminothiazole monohydrobromide was purchased from Thermoscientific, triphenylphosphine was purchased from Fluka and 4-Hydroxycoumarin has been acquired from Apollo Scientific. Solvents were purchased from Fisher Chemical, Acros Organics and Honeywell. All reagents and solvents were used without further purification. 7-hydroxycoumarincarbonylamino-d-alanine (HADA) was prepared according to a published procedure. [67] Unless otherwise noted, solvents used in the preparation of all molecules were dry and O_2-free. All manipulations were performed under a nitrogen atmosphere. Thin layer chromatography (TLC) was performed on TLC Plates ALUGRAM® Xtra SIL G / UV_{254} (0.20 mm layer thickness). Silica gel for chromatography was prepared with silica (60 Å particle size, 35-70 µm mesh). For determination of the cytotoxicity, Dulbecco's Modified Eagle Medium (DMEM) (with L-glutamine and glucose) and trypsin-EDTA were purchased from Sigma. L-

glutamine penicillin/streptomycin (l-glu pen-strep) were purchased from Pan. Thiazolyl blue tetrazolium bromide (MTT) was provided Thermoscientific – Acros. Fetal bovine serum (FBS) and phosphate buffered saline (PBS, pH 7.4, 1X) solution was obtained from Gibco. 96-Well plates were purchased from Sarstedt. MCF-7 – breast cancer cell line, HCT116 – human colon cancer cell line, A549 – lung carcinoma cell line and L929 – mouse fibroblast cells were kindly gifted from Prof. David Hoogewijs, Department of Medicine, University of Fribourg, Switzerland. For SAXS studies, 1-palmitoyl-2-oleoyl-sn-glycero-3-phospho-(1'-rac-glycerol) (sodium salt) (POPG, purity > 99%, Avanti Polar Lipids, Alabaster, USA) and 1-palmitoyl-2-oleoyl-sn-glycero-3-phosphoethanolamine (POPE, purity > 99%, Avanti Polar Lipids, Alabaster, USA), $CHCl_3$ (99.0-99.4%, Honeywell, Germany), PBS, 1x pH 7.4, containing 137 mM NaCl (Acros Organics, 99.5% purity, Denmark), 2.7 mM KCl (Carl Roth, Karlsruhe, Germany), 10.1 mM Na_2HPO_4 $2H_2O$ (Sigma–Aldrich, Steinheim, Germany), and 1.8 mM KH_2PO4 (Sigma–Aldrich, Steinheim, Germany) were used. The rhenium complexes were dissolved in DMSO (Acros Organics, 99.7 %purity, USA).

4.2. Instruments and analysis

Bruker Advance III 500 MHz (AV500) and Bruker Advance III 400 MHz were used to record the ^{1}H and ^{13}C NMR spectra. The corresponding chemical shifts were reported in ppm referenced to residual solvent signals. A Bruker TENSOR II was employed to acquire IR spectra with the following settings: 16 background scans, 32 sample scans, and a resolution of 4 cm^{-1} in the 4000-400 cm^{-1} range. A Jasco V730 spectrophotometer was used to record UV-Vis spectra. The fluorescence emission was carried out on Perkin Elmer LS-50B Luminescence Spectrometer. FreeZone Plus 4.5 Liter Cascade Benchtop Freeze Dry System was used to lyophilize the samples. A a Stoe STADIVARI diffractometer (CuKα1 (λ = 1.5406 Å)) fitted with an Oxford Cryosystems cryostat, collected single crystal diffraction data of the compounds. The structures were solved using Intrinsic Phasing in the ShelXT structure solution program and refined using Least Squares minimization in the ShelXL refinement software. All crystal structures in this study have been deposited at Cambridge Crystallographic Data Center. CCDC numbers 2375721-2375724, 2375733-2375743 and 2375745 contain the supplementary crystallographic data for this paper.

SAXS measurements were conducted on the SAXSpoint 5.0 (Anton Paar, Graz, Austria) coupled to a MetalJet D2 X-ray source (Excillum, Kista, Sweden). The samples were filled into borosilicate capillaries with 1.5 mm diameter (Hilgenberg, Germany) which were loaded into a thermostatic sample holder (Anton Paar, Graz, Austria). An X-ray beam with a wavelength, λ, of 0.134 nm (9.3keV) and sample-to-detector distance was 600 mm was used. This provides a scattering vector magnitude (q)-range from 0.1 – 6.6 nm^{-1}. The scattering vector magnitude q was calculated with Eq. 1, where n is the refractive index, which is virtually unity for X-rays in this study, θ is the scattering angle.

$$q = \frac{4\pi n}{\lambda} \sin\left(\frac{\theta}{2}\right) \quad \text{Eq. 1}$$

The 2-dimensional SAXS patterns were recorded using a 2D EIGER R 1M detector (Dectris Ltd., Baden, Switzerland) with a total area of 77.1 × 79.65 mm^2 and pixel size of 75 × 75 μm^2. The patterns were radially integrated into the 1-dimensional I(q) functions using SAXS analysis

4.20 (Anton Paar, Graz, Austria). The temperature was varied according to the sample. Measurements were done in sets of 12 to check for beam damage, and the average of the results was used. No beam damage was observed. The scattering curves were corrected for transmittance. Buffer scattering was measured with all samples and subtracted as background from the scattering curves.

The SAXS curves of the vesicles were analyzed with the random lamellar bilayer stack model, modified with the Caillé theory [68] that has been used previously for similar vesicle model systems. [69]

4.3. Synthetic procedures

Ligands **L1**-**L6** were prepared according to procedures previously described, [39-41] adapted to our needs. Briefly, derivatives of 2-amino thiazole (1.0 equiv., 1 mmol) were dissolved in 3 mL H_2O, followed by the addition of 5 mL of 6 M HCl (0.5 mL concentrated H_2SO_4 was used for **L3** and **L5**). The system was cooled and kept at - 5 °C to 0 °C using the ice-salt bath. Thereafter, an aqueous solution of 0.7 mL $NaNO_2$ (10 *wt*.) was added slowly dropwise and stirred vigorously on a magnetic stirrer for 1h. After 1 h, a fresh solution of 4-hydroxycoumarin (1.0 equiv., 1 mmol) in 3 mL NaOH (10 *wt.)* was added. Red-orange precipitates were obtained, which were stirred for 1 h in the ice bath and 1h at room temperature. The precipitate was then vacuum-filtered and water-rinsed. The resulting product was then suspended in a solvent mixture of 2:1 (v/v) ethanol: water, subjected to ultrasonication for a period (5 min) and subsequently left to stand for an appropriate time to permit the formation of a precipitate. The precipitate was collected by vacuum filtration and dried under a Schlenk line vacuum for the next stage. Complexes **1**-**6** were prepared according to the following general procedure. [38] $[Re(CO)_5Br]$ (123 µmol, 1.0 equiv.) and the corresponding ligand (135 µmol, 1.1 equiv.) were suspended in 3 mL dry toluene and heated up at 84 °C in oil bath, overnight. A black precipitate was obtained and collected by vacuum filtration. The precipitate was rinsed with 10 mL of dry toluene and then dried under a Schlenk line vacuum for further characterization. No additional purification was necessary. Complexes **7**-**16** were synthesized as follows. $[Re(CO)_5Br]$ (123 µmol, 1.0 equiv.) the corresponding ligands (i.e. **L1**-**L6** and L#, 123 µmol, 1.0 equiv.) and KPF_6 (738.6 µmol, 6.0 equiv.) were suspended and refluxed in 7 mL of MeOH overnight. After overnight reaction the mixture was evaporated and the crude was purified by column chromatography using ethyl acetate:pentane as an eluent. For complex **7** a ratio of 90:10 ethyl acetate:pentane was used. For complexes **8**-**15** a ratio of 70:30 ethyl acetate:pentane was used, and for **16** a ratio 50:50 ethyl acetate:pentane was used. After the evaporation and lyophilization of the separated fractions containing the complexes, dark red dry powders were collected.

***fac*-[Re(CO)$_3$(L1)Br] (1).** Black powder, yield 92.39%. ^{1}H NMR (500 MHz, CD_2Cl_2) δ 11.21 (s, 1H), 8.30 (dd, J = 3.36, 13.43 Hz, 2H), 8.14 (dd, J = 1.22, 7.93 Hz, 1H), 7.75 - 7.80 (m, 1H), 7.44 - 7.49 (m, 2H). ^{13}C (500 MHz, CD_2Cl_2) δ 115.22, 117.59, 125.59, 125.75, 126.05, 131.25, 136.04, 143.42, 153.78, 156.64, 160.32, 176.75. IR, υ (CO) symmetric 1906 cm^{-1} and asymmetric stretching at 2015 cm^{-1}. UV - Vis (in CH_2Cl_2) λ_{max} $^{AB\ [nm]}$ 560, 505, 481, 360, 295, 257.

***fac*-[Re(CO)$_3$(L2)Br] (2).** Black powder, yield 92.82%. ^{1}H NMR (500 MHz, CD_2Cl_2) δ 10.83 - 10.89 (s, 1H), 8.12 (dd, *J* = 1.22, 7.93 Hz, 1H), 8.04 - 8.07 (m, 1H), 7.74 - 7.78 (m, 1H), 7.43 - 7.47 (m, 2H), 2.75 (s, 3H). Due to its precipitation, ^{13}C NMR spectra could not be obtained for this compound. IR, υ (CO) symmetric 1931 cm^{-1} and asymmetric stretching at 2018 cm^{-1}. UV - Vis (in CH_2Cl_2) λ_{max} $^{AB\ [nm]}$ 526, 487, 394, 298, 261.

***fac*-[Re(CO)$_3$(L3)Br] (3).** Black powder, yield 67.16%. ^{1}H NMR (500 MHz, CD_2Cl_2) δ 10.49 (s, 1H), 8.12 (dd, *J* = 1.14, 7.86 Hz, 1H), 8.01 (s, 1H), 7.73 - 7.78 (m, 1H), 7.43 - 7.48 (m, 2H), 2.82 (s, 3H). ^{13}C (500 MHz, CD_2Cl_2) δ 196.3, 192.9, 180.9, 176.2, 159.2, 156.5, 155.3, 153.6, 135.6, 126.8, 125.8, 125.6, 125.2, 117.5, 115.2, 20.3. IR, υ (CO) symmetric 1906 cm^{-1} and asymmetric stretching at 2019 cm^{-1}. UV - Vis (in CH_2Cl_2) λ_{max} $^{AB\ [nm]}$ 520, 486, 374, 296, 260.

***fac*-[Re(CO)$_3$(L4)Br] (4).** Black powder, yield 83.51%. ^{1}H NMR (500 MHz, CD_2Cl_2) δ 11.35 - 11.41 (s, 1H), 8.27 (s, 1H), 8.12 - 8.16 (m, 1H), 7.76 - 7.81 (m, 1H), 7.42 - 7.49 (m, 2H). Due to its precipitation, ^{13}C NMR spectra could not be obtained for this compound. IR, υ (CO) symmetric 1945 cm^{-1} and asymmetric stretching at 2022 cm^{-1}. UV – Vis (in CH_2Cl_2) λ_{max} $^{AB\ [nm]}$ 522, 496, 376, 268.

***fac*-[Re(CO)$_3$(L5)Br] (5).** Black powder, yield 81.42%. ^{1}H NMR (500 MHz, CD_2Cl_2) δ 12.37 - 12.53 (s, 1H), 8.42 (d, *J* = 8.24 Hz, 1H), 8.13 - 8.21 (m, 2H), 7.87 - 7.92 (m, 1H), 7.79 - 7.86 (m, 2H), 7.46 - 7.51 (m, 2H). ^{13}C (500 MHz, CD_2Cl_2) δ 197.0, 192.5, 182.9, 174.8, 161.9, 156.7, 154.0, 149.1, 137.0, 137.7, 136.7, 130.6, 130.4, 126.8, 126.5, 125.9, 124.8, 124.3, 117.7, 115.2. IR, υ (CO) symmetric 1916 cm^{-1} and asymmetric stretching at 2015 cm^{-1}. UV Vis (in CH_2Cl_2) λ_{max} $^{AB\ [nm]}$ 534, 504, 396, 296.

***fac*-[Re(CO)$_3$(L6)Br] (6).** Black powder, yield 71.91%. ^{1}H NMR (500 MHz, CD_2Cl_2) δ 10.23 (,s 1H), 8.10 (dd, *J* = 0.99, 7.86 Hz, 1H), 7.71 - 7.77 (m, 1H), 7.41 - 7.48 (m, 2H), 2.72 (s, 3H), 2.67 (s, 3H). ^{13}C (500 MHz, CD_2Cl_2) δ 196.6, 193.1, 181.1, 172.1, 158.6, 156.6, 153.4 152.1, 143.5, 135.2, 125.6, 125.5, 117.4, 115.3, 18.1, 14.6. IR, υ (CO) symmetric 1946 cm^{-1} and asymmetric stretching at 2019 cm^{-1}. UV Vis (in CH_2Cl_2) λ_{max} $^{AB\ [nm]}$ 526, 480, 395, 297, 259.

***fac*-[Re(CO)$_3$(L1)py] (7).** Dark red powder, yield 36.59 %. ^{1}H NMR (400 MHz, CD_3CN) d 8.70 - 8.72 (m, 2H), 8.20 - 8.23 (m, 1H), 7.91 (tt, *J* = 1.59, 7.70 Hz, 1H), 7.74 - 7.79 (m, 2H), 7.45 (d, *J* = 3.42 Hz, 1H), 7.37 - 7.42 (m, 3H), 7.29 (td, *J* = 0.55, 7.83 Hz, 1H). ^{13}C NMR (101 MHz, CD_3CN) d 166.1, 159.7, 154.6, 153.3, 142.1, 140.8, 137.1, 128.5, 127.4, 125.9, 121.4. IR υ (CO) symmetric 1889 and 1909 cm^{-1} and asymmetric stretching at 2017 cm^{-1}. UV Vis (in CH_3CN) λ_{max} $^{AB\ [nm]}$ 502, 389, 261.

***fac*-[Re(CO)$_3$(L2)py] (8).** Dark red powder, yield 59.55%. ^{1}H NMR (400 MHz, CD_3CN) d 8.70 - 8.72 (m, 2H), 8.20 (dd, *J* = 1.34, 7.95 Hz, 1H), 7.91 (tt, *J* = 1.59, 7.70 Hz, 1H), 7.73 - 7.77 (m, 1H), 7.48 (q, *J* = 1.18 Hz, 1H), 7.37 - 7.42 (m, 3H), 7.29 (dd, *J* = 0.61, 8.31 Hz, 1H), 2.45 (d, *J* = 1.22 Hz, 3H) ^{13}C NMR (101 MHz, CD_3CN) d 153.9, 152.8,140.2, 139.3, 136.2, 127.9, 126.8, 125.3, 125.1, 12.22. IR υ (CO) symmetric 1890 and 1917 cm^{-1} and asymmetric stretching at 2018 cm^{-1}. UV Vis (in CH_3CN) λ_{max} $^{AB\ [nm]}$ 499, 406, 260.

***fac*-[Re(CO)$_3$(L3)py] (9).** Dark red powder, yield 68.63%. ^{1}H NMR (400 MHz, CD_3CN) d 8.74 - 8.76 (m, 2H), 8.22 (dd, *J* = 1.59, 7.95 Hz, 1H), 7.92 (tt, *J* = 1.59, 7.70 Hz, 1H), 7.74 - 7.78 (m, 1H), 7.37 - 7.43 (m, 3H), 7.29 (dd, *J* = 0.61, 8.31 Hz, 1H), 7.02 (d, *J* = 0.98 Hz, 1H), 2.46 (d, *J* = 0.98 Hz, 3H) ^{13}C NMR (101 MHz, CD_3CN) d 178.9, 165.4, 153.9, 152.8, 151.8, 140.2, 136.2, 128.1, 126.8, 125.3, 17.2 IR υ (CO) symmetric 1905 cm^{-1} and asymmetric stretching at 2018 cm^{-1}. UV Vis (in CH_3CN) λ_{max} $^{AB\ [nm]}$ 500, 412, 260.

***fac*-[Re(CO)$_3$(L4)py] (10).** Dark red powder, yield 46.62%. ^{1}H NMR (400 MHz, CD_3CN) d 8.65 - 8.67 (m, 2H), 8.21 (dd, *J* = 1.65, 8.01 Hz, 1H), 7.92 (tt, *J* = 1.59, 7.70 Hz, 1H), 7.75 - 7.80 (m, 2H), 7.37 - 7.42 (m, 3H), 7.28 (d, *J* = 8.31 Hz, 1H). Due to its precipitation, ^{13}C NMR spectra could not be obtained for this compound. IR υ (CO) symmetric 1893 and 1916 cm^{-1} and asymmetric stretching at 2019 cm^{-1}. UV Vis (in CH_3CN) λ_{max} $^{AB\ [nm]}$ 504, 405, 261.

***fac*-[Re(CO)$_3$(L5)py] (11).** Dark red powder, yield 35.95%. ^{1}H NMR (400 MHz, CD_3CN) d 8.74 - 8.76 (m, 2H), 8.25 (dd, *J* = 1.34, 7.95 Hz, 1H), 7.98 - 8.01 (m, 1H), 7.88 - 7.94 (m, 2H), 7.77 - 7.81 (m, 1H), 7.53 (ddd, *J* = 1.34, 7.18, 8.22 Hz, 1H), 7.38 - 7.48 (m, 4H), 7.30 (dd, *J* = 0.61, 8.31 Hz, 1H). Due to its precipitation, ^{13}C NMR spectra could not be obtained for this compound. IR υ (CO) symmetric 1923 cm^{-1} and asymmetric stretching at 2018 cm^{-1}. UV Vis (in CH_3CN) λ_{max} $^{AB\ [nm]}$ 496, 403, 261.

***fac*-[Re(CO)$_3$(L6)py] (12).** Dark red powder, yield 31.38%. ^{1}H NMR (400 MHz, CD_3CN) d 8.75 (dd, *J* = 1.59, 6.48 Hz, 2H), 8.21 (dd, *J* = 1.71, 7.95 Hz, 1H), 7.91 (tt, *J* = 1.57, 7.72 Hz, 1H), 7.75 (ddd, *J* = 1.65, 7.12, 8.47 Hz, 1H), 7.36 - 7.43 (m, 3H), 7.29 (dd, *J* = 0.61, 8.31 Hz, 1H), 2.34 - 2.36 (m, 6H). Due to its precipitation, ^{13}C NMR spectra could not be obtained for this compound. IR υ (CO) symmetric 1891 and 1914 cm^{-1} and asymmetric stretching at 2017 cm^{-1}. UV Vis (in CH_3CN) λ_{max} $^{AB\ [nm]}$ 514, 418, 260.

***fac*-[Re(CO)$_3$(L1)L#] (where L# = 1-methylimidazole, 13)** Dark red powder, yield 56.44%. ^{1}H NMR (400 MHz, CD_3CN) d 8.13 (dd, *J* = 1.34, 7.95 Hz, 1H), 7.73 - 7.77 (m, 3H), 7.42 (d, *J* = 3.42 Hz, 1H), 7.37 (ddd, *J* = 1.04, 7.18, 8.04 Hz, 1H), 7.30 (dd, *J* = 0.61, 8.44 Hz, 1H), 7.01 (t, *J* = 1.41 Hz, 1H), 6.95 (t, *J* = 1.53 Hz, 1H), 3.57 (s, 3H) ^{13}C NMR (101 MHz, CD_3CN) d 141.9, 141.9, 136.6, 130.5, 128.4, 125.8, 123.3, 121.2, 120.3, 35.1. IR υ (CO) symmetric 1990 cm^{-1} and asymmetric stretching at 2017 cm^{-1}. UV Vis (in CH_3CN) λ_{max} $^{AB\ [nm]}$ 498, 389, 259.

***fac*-[Re(CO)$_3$(L1)L#] (where L# = benzylamine, 14)** Dark red powder, yield 50.89%. ^{1}H NMR (400 MHz, CD_3CN) d 8.08 (dd, *J* = 1.47, 7.95 Hz, 1H), 7.74 - 7.79 (m, 2H), 7.45 (d, *J* = 3.42 Hz, 1H), 7.38 (ddd, *J* = 1.04, 7.21, 8.01 Hz, 1H), 7.33 (dd, *J* = 0.61, 8.44 Hz, 1H), 7.25 - 7.30 (m, 5H), 4.10 - 4.17 (m, 1H), 3.94 - 4.04 (m, 2H), 3.67 (d, *J* = 8.19 Hz, 1H). ^{13}C NMR (101 MHz, CD_3CN) d 180.8, 167.4, 160.1, 154.5, 142.1, 140.4, 136.6, 129.6, 129.1, 128.8, 128.4, 126.4, 125.7, 120.9, 52.3. IR υ (CO) symmetric 1893 and 1950 cm^{-1} and asymmetric stretching at 2017 cm^{-1}. UV Vis (in CH_3CN) λ_{max} $^{AB\ [nm]}$ 453, 392, 263.

***fac*-[Re(CO)$_3$(L1)L#] (where L# = 2-aminothiazole, 15)** Dark red powder, yield 68.63%. ^{1}H NMR (400 MHz, CD_3CN) d 8.21 (dd, *J* = 1.59, 7.95 Hz, 1H), 7.75 - 7.80 (m, 2H), 7.47 (d, *J* = 3.55 Hz, 1H), 7.38 (dt, *J* = 0.98, 7.64 Hz, 1H), 7.30 (dd, *J* = 0.67, 8.38 Hz, 1H), 7.02 (d, *J* =

4.16 Hz, 1H), 6.94 - 6.99 (m, 2H), 6.50 (d, *J* = 4.28 Hz, 1H). ^{13}C NMR (101 MHz, CD_3CN) d 141.5, 139.3, 136.9, 128.4, 125.9, 121.7, 108.8. IR υ (CO) symmetric 1898 cm^{-1} and asymmetric stretching at 2019 cm^{-1}. UV Vis (in CH_3CN) λ_{max} $^{AB\ [nm]}$ 501, 418, 257.

***fac*-[Re(CO)$_3$(L1)L#] (where L# = triphenylphosphine, 16)** Dark red powder, yield 25.23%. ^{1}H NMR (400 MHz, CD_3CN) d 7.95 (dd, *J* = 1.53, 8.01 Hz, 1H), 7.69 - 7.73 (m, 1H), 7.61 (d, *J* = 3.42 Hz, 1H), 7.29 - 7.45 (m, 17H), 7.23 (dd, *J* = 0.67, 8.38 Hz, 1H) ^{13}C NMR (101 MHz, CD_3CN) 180.3, 179.9, 166.3, 159.3, 154.3, 141.2, 136.6, 134.6, 134.5, 134.4, 134.3, 132.1, 131.9, 131.9, 131.7, 131.6, 129.8, 129.7, 128.4, 125.5, 121.2, 119.9 IR υ (CO) symmetric 1905 and 1935 cm^{-1} and asymmetric stretching at 2025 cm^{-1}. UV Vis (in CH_3CN) λ_{max} $^{AB\ [nm]}$ 507, 392, 259.

4.3. Biological studies

The cytotoxicity of the complexes was tested in MCF-7 – breast cancer cell line, HCT116 – human colon cancer cell line, A549 – lung carcinoma cell line and L929 – mouse fibroblast cells in DMEM medium supplemented with 10% v/v FBS and 1% v/v pen/strep with l-glu. For the test, the common MTT assay was used. Briefly, cells were seeded to 96-well plate in $3.75x10^4$ cell /mL concentration for L929 cells and $5x10^4$ cell /mL concentration for cancer cells for 24 hours. Then, complexes, dissolved in DMSO, were diluted with medium and injected to wells in 10-0.63 μM concentration range. After 24 hours incubation, MTT solution (5mg/mL in PBS) in fresh medium was added to the wells in 25% volume ratio and plates incubated for 4 hours. Then, the formazan crystals, resulting from the mitochondrial activity in live cells, were dissolved in a DMSO:EtOH (1:1 v/v) solution. Control cells were not exposed to complexes, but only DMSO 1% v/v. 100% viability is assumed for the control cells. The relative cell viability was calculated by making ratio with control cells. Statistical analysis of the bioactivities of complexes were conducted by using ordinary one-way ANOVA analysis of variance followed by multiple Dunnett's comparison test of GraphPad Prism 9 software package. All measurements were expressed as mean values ± standard deviation (SD). $p < 0.05$ was accepted as statistically significant difference. Statistical significance: (*) $p < 0.0332$, (**) $p < 0.021$, (***) $p < 0.0002$, (****) $p < 0.0001$. IC_{50} values in cell cytotoxicity experiment were evaluated by using nonlinear regression analysis followed by variable slope. For determination of the cytotoxicity, Tecan – Infinity M Nano was used with iControl program.

Antimicrobial activity was evaluated against *S. aureus* MRSA43300 (methicillin-resistant) and *S. aureus* ATCC25923 (methicillin-sensitive) and two fungi (*Candida albicans* SC5314) and *C. auris 7* (a clinical strain)). All reference strains were obtained from the American Type Culture Collection (ATCC) and the National Collection of Type Cultures (NCTC), while a clinical *C. auris* strain 7 was kindly provided by Dr Aleksandra Barac (University Clinical Center of Serbia) and prof. Cornelia Lass-Floerl (University of Innsbruck). Prior to each experiment, frozen stocks in 20% glycerol at -80 °C were thawed and inoculated onto solid Yeast-Potato Dextose (YPD) plates (fungi) or Lauria (LA) agar plates (bacteria), and cultured at 37 °C for 24-48 h. *In vitro* antimicrobial activity determination was evaluated as previously reported. [34] The checkboard assay was performed to check the possible synergistic effect of

complexes **2** and **6** with vancomycin, an active antibiotic for Gram (+) strains. For the test, the reference procedure was followed.

***In vivo* toxicity zebrafish (*Danio rerio*) model** and efficacy in the zebrafish-*S. aureus* ATCC43300 model of infection of **2** and **6** was carried in the according to a previously published procedure [34] following the general rules of the OECD Guidelines for the Testing of Chemicals (OECD, 2013, Test No. 236). All experiments involving zebrafish were performed in compliance with the European directive 2010/63/EU and the ethical guidelines of the Guide for Care and Use of Laboratory Animals of the Institute of Molecular Genetics and Genetic Engineering, University of Belgrade.

The effect of complexes on synthesis of peptidoglycan wall was tested by HADA staining according to Mendes et al. [35] For this experiment, the *S. aureus* ATCC25923 strain was grown to a OD600 of 0.4. Aliquots of 200 µL of the bacterial culture were treated with 0.5%DMSO (negative control), 2× and 4×MIC of samples and incubated for 10 minutes at 37°C in 250 rpm shaker. Then, tubes were centrifuged, 155 µL supernatant was discarded and 5 µL HADA (1 mM) was added. Bacteria were incubated with HADA for 5 minutes at 37°C. To terminate the staining process, 500 µL ice-cold 1x PBS was added to tubes which were then washed three times with cold PBS. The bacteria were suspended in water and transferred to agarose layer. HADA staining was observed under microscope by excitation at 405 nm and emission at 450 nm. Quantification of fluorescence of the HADA staining was performed by using ImageJ program. The fluorescence intensity was normalized with following formula (n=3):

$$Normalized\ intensity\ (\%) = \frac{Intensity\ (a.u.)/\#\ of\ bacteria}{Average\ (Intensity\ in\ DMSO\ (a.u.)/\#\ of\ bacteria\ in\ DMSO)}\ x\ 100$$

The checkboard assay experiment was performed to check the synergistic effect with Vancomycin, active antibiotic for Gram (+) strains. For the test, the reference procedure was followed [70]. Briefly, 50 µL of 2X CAMHB medium injected to all well in 96 well plate. 50 µL of 40 µg/mL Vancomycin was injected to A1 to A11 well in 96-well plate. 50 µL of 80 µg/mL Vancomycin (50 mg/mL stock solution in DMSO) was injected to A12 well in 96-well plate. There was performed the serial dilution until G-row. Then, 50 µL of 4X highest concentration of the complexes were injected to A12 to H12 well in 96-well plate. The serial dilution was performed until Column 2. *S. Aureus* strain growth overnight in 1X MHB medium was prepared in OD600 of 0.14 concentration. Then, the bacteria stock diluted in 0.9% NaCl in 1 to 200 times to obtain 10^6 CFU/mL concentration. 50 µL of bacteria stock injected to all wells of 96-well plate. After 24 h incubation at 37°C incubator, the absorbance of bacteria at 600 nm was measured with plate reader. The H1-well of 96-well plate was used as bacteria control.

The time dependent membrane potential measurement was performed with the 3,3′-diethyloxacarbocyanine iodide ([$DiOC_2(3)$], Sigma) membrane stain on *S. Aureus* ATCC25923 strain according to the reported procedure. [35] Briefly, bacteria were grown to a OD600 concentration of 0.5, treated with 30 µM [$DiOC_2(3)$] (3 mM stock solution in DMSO) for 15 minutes at 37°C and dark. After 15 minutes, stained bacteria were transferred into a black 96-well plate. The wells were read via a microplate reader for 3 minutes to acquire the baseline. Then, the bacteria were treated with 1% DMSO (negative control), CCCP (carbonyl cyanide m-chlorophenyl hydrazone, 25 µM, 2×MIC, positive control,) and different concentration of complexes (1×, 2× and 4×MIC) for 15 minutes. The red (λ_{exc}: 485 nm, λ_{em}: 635 nm) and green (λ_{exc}: 485 nm, λ_{em}: 530 nm) emissions of [$DiOC_2(3)$] were the recorded every minute. Emission

data were normalized according to the negative control and the ratio of normalized red to normalized green was plotted.

Propidium iodide (PI) was used to measure the effect of complexes on the membrane integrity of bacteria. *S. aureus* MSSA25923 bacteria were grown overnight, diluted to a OD600 of 0.3. and then 1 mL of culture was transferred to Eppendorf tubes. Bacteria were treated with 1% DMSO, 100 µg/mL Nisin (10 mg/mL stock solution in DMSO) and 0.5×, 1×, 2× and 4×MIC concentrations of samples. Bacteria samples were incubated separately for 30 minutes, 2 hours and 4 hours at 37°C by shaking. After every time interval, 10 µg/mL PI solution (1 mg/mL stock solution in DMSO) was injected, and tubes incubated 5 minutes. Then, bacteria were washed with prewarmed 1x PBS two times. After the washing steps, bacteria were suspended in 1x PBS and transferred to black 96-well plate as three replicas. The emission of the PI at 625 nm was recorded via plate reader with excitation at 485 nm. For evaluation of PI staining under microscope, bacteria strains were incubated with 2×MIC of complexes for 4 hours. After the incubation, tubes were incubated with 10 µg/mL PI solution for 5 minutes at 37°C. Then, bacteria were washed and fixed with 1:3 v/v acetic acid: methanol mixture for 30 minutes. After fixation, bacteria were suspended in sterile water and transferred to 1% agarose layer for imaging process.

Membrane mimetic vesicle preparation

Vesicle preparation and interaction studies. Bacteria membrane mimetic vesicles were prepared with 1-palmitoyl-2-oleoyl-sn-glycero-3-phospho-(1'-rac-glycerol) (sodium salt) (POPG) and 1-palmitoyl-2-oleoyl-sn-glycero-3-phosphoethanolamine (POPE) using the established thin film method A POPG:POPE weight ratio of 3:1 is characteristic for gram-positive membrane models (g^+) In short, 7.5 mg of POPG and 2.5 mg of POPE (mass ratio of 3:1) were dissolved in 1 mL of in a 10 mL round flask. $CHCl_3$ was then evaporated in a rotary evaporator for at least 4 hours and dried overnight under vacuum. The phospholipid film in the round flask was then rehydrated with phosphate buffered saline (PBS) 2.7 mM KCl, 10.1 mM Na_2HPO_4 $2H_2O$) and 1.8 mM KH_2PO_4. Vesicle formation was achieved by vortexing and ultrasonication for 10 min to achieve vesicle solutions of 1wt% (POPG and POPE in PBS). The flasks and the buffer were kept at 25 °C during the hydration process. The rhenium complex were dissolved in DMSO to gain 100 mg/ml stock solutions and mixed to the g^+ vesicles to at a phospholipid:complex mass ratio of 10:1 of lipids to complexes.

4.5. Theoretical Calculations

DFT calculations were performed with the hybrid meta-GGA functional wB97XD [71-74] in combination with the standard SDD basis sets.[75]The optimized structures were subject to frequency analysis to verify that they represented minima on the potential energy surface. All calculations were performed with Gaussian 09 software (version 5.0.9, Carnegie Mellon University, Gaussian, Inc.). Conformation calculations were performed as previously [32] using the AutoDock Vina version 1.2.0 (The Scripps Research Institute, La Jolla, San Diego, USA) and AutoDock4 version 4.2.6 (AD4, The Scripps Research Institute, La Jolla, San Diego, USA) softwares. Figures were prepared with the AutoDockTools software (version 1.5.7, The Scripps Research Institute, La Jolla, San Diego, USA). The xyz coordinates of complexes **2** and **6** were taken from the crystal structure of the same. Due to the fact that AD4 failed to assign a change to the metal ion, a charge of 0.320 (to Re) was assigned to the atom by editing the

corresponding .PDBQT file. The POPE membrane model (fully equilibrated at 303K in H_2O) prepared by Jämbeck and Lyubartsev (made available at http://www.fos.su.se/~sasha/SLipids/Downloads.html) was used to prepare the semi-flexible 1:2 POPE:POPG membrane model in the conformation analysis. Six central lipids were selected as fully flexible (ca. 270 unlocked rotatable bonds), forming an area of ca. 400 $Å^2$ (viewed from the top of the membrane facing the cellular exterior). The search space was defined by a box wrapped around the space the receptors or the fully flexible lipids that also included rigid lipid units. For the membrane model, the search space was defined by a volume on 38640 $Å^3$. The number of modes and the exhaustiveness parameter were set to 40 and 10 for the calculations. Such parameters were deemed sufficient for the calculations' accuracy. [76-78]

Author contributions

F.R. carried out the synthesis, purification and characterization of all ligands and complexes and the *in vitro* cytotoxicity cell studies for compounds **13-16**. G.D. performed *in vitro* cell cytotoxicity experiments for **1-12** complexes, mechanisms of action studies (HADA, checkboard assay, [$DiOC_2(3)$] membrane potential and PI membrane integrity for **2** and **6**). N.P. and A.P. performed *in vitro* MICs studies in bacteria and candida strains, for complexes **1-16** and *in vivo* studies for **2** and **6**. B.T. performed SAXS experiments on **2** and **6** under the supervision of S.S. A.C. carried out all crystallographic analysis and data refinement. Y.C. prepared HADA. F.Z. executed theoretical calculations. F.R., G.D., N.P. and B.T. wrote their respective sections. S.S., A.P. and F.Z. provided scientific guidance and edited the manuscript. A.P. and F.Z. conceived and directed the study. All authors have read and approved the manuscript.

Acknowledgements

F.R. is obliged to the Swiss Federal Commission for Scholarships for Foreign Students (FCS) and the University of Fribourg, Switzerland for financial support. Support from the Centenary Research Fund (FC-23-901) of the University of Fribourg is gratefully acknowledged (F.Z.). S.S. acknowledges SNSF project number IZBRZ2_186251. This work was supported by University of Fribourg and Ministry of Science, Technological Development and Innovation of the Republic of Serbia, 451-03-66/2024-03/200042, 2024.

References

[1] M. Woolhouse, C. Waugh, M.R. Perry, H. Nair, Global disease burden due to antibiotic resistance - state of the evidence, J Glob Health, 6 (2016) 010306.
[2] S.B. Levy, B. Marshall, Antibacterial resistance worldwide: causes, challenges and responses, Nat. Med, 10 (2004) S122-129.
[3] A.S. Abd-El-Aziz, C. Agatemor, N. Etkin, Antimicrobial resistance challenged with metal-based antimicrobial macromolecules, Biomaterials., 118 (2017) 27-50.
[4] E. Christaki, M. Marcou, A. Tofarides, Antimicrobial Resistance in Bacteria: Mechanisms, Evolution, and Persistence, J. Mol. Evol., 88 (2020) 26-40.

[5] D. Chinemerem Nwobodo, M.C. Ugwu, C. Oliseloke Anie, M.T.S. Al-Ouqaili, J. Chinedu Ikem, U. Victor Chigozie, M. Saki, Antibiotic resistance: The challenges and some emerging strategies for tackling a global menace, J. Clin. Lab. Anal., 36 (2022) e24655.
[6] WHO's List of Medically Important Antimicrobials: a risk management tool for mitigating antimicrobial resistance due to non-human use. Geneva: World Health Organization; 2024. Licence: CC BY-NC-SA 3.0 IGO.
[7] A. Sychrová, I. Kolářiková, M. Žemlička, K. Šmejkal, Natural compounds with dual antimicrobial and anti-inflammatory effects, Phytochem. Rev. , 19 (2020) 1471-1502.
[8] D.M.P. De Oliveira, B.M. Forde, T.J. Kidd, P.N.A. Harris, M.A. Schembri, S.A. Beatson, D.L. Paterson, M.J. Walker, Antimicrobial Resistance in ESKAPE Pathogens, Clin. Microbiol. Rev., 33 (2020).
[9] C.D. Salgado, B.M. Farr, D.P. Calfee, Community-acquired methicillin-resistant Staphylococcus aureus: a meta-analysis of prevalence and risk factors, Clin. Infect. Dis., 36 (2003) 131-139.
[10] B.C. Herold, L.C. Immergluck, M.C. Maranan, D.S. Lauderdale, R.E. Gaskin, S. Boyle-Vavra, C.D. Leitch, R.S. Daum, Community-acquired methicillin-resistant Staphylococcus aureus in children with no identified predisposing risk, JAMA., 279 (1998) 593-598.
[11] F.R. DeLeo, M. Otto, B.N. Kreiswirth, H.F. Chambers, Community-associated meticillin-resistant Staphylococcus aureus, Lancet, 375 (2010) 1557-1568.
[12] E.J. Gorak, S.M. Yamada, J.D. Brown, Community-acquired methicillin-resistant Staphylococcus aureus in hospitalized adults and children without known risk factors, Clin. Infect. Dis., 29 (1999) 797-800.
[13] F.M. Hussain, S. Boyle-Vavra, R.S. Daum, Community-acquired methicillin-resistant Staphylococcus aureus colonization in healthy children attending an outpatient pediatric clinic, Pediatr. Infect. Dis. J., 20 (2001) 763-767.
[14] A.J. Kallen, T.J. Driscoll, S. Thornton, P.E. Olson, M.R. Wallace, Increase in community-acquired methicillin-resistant Staphylococcus aureus at a Naval Medical Center, Infect.Control Hosp. Epidemiol., 21 (2000) 223-226.
[15] M. Bassetti, E. Nicco, M. Mikulska, Why is community-associated MRSA spreading across the world and how will it change clinical practice?, Int. J. Antimicrob. Agents 34 (2009) S15-S19.
[16] A. Frei, J. Zuegg, A.G. Elliott, M. Baker, S. Braese, C. Brown, F. Chen, C. G. Dowson, G. Dujardin, N. Jung, A.P. King, A.M. Mansour, M. Massi, J. Moat, H.A. Mohamed, A.K. Renfrew, P.J. Rutledge, P.J. Sadler, M.H. Todd, C.E. Willans, J.J. Wilson, M.A. Cooper, M.A.T. Blaskovich, Metal complexes as a promising source for new antibiotics, Chem. Sci. J., 11 (2020) 2627-2639.
[17] F. Li, J.G. Collins, F.R. Keene, Ruthenium complexes as antimicrobial agents, Chem. Soc. Rev., 44 (2015) 2529-2542.
[18] M. Patra, G. Gasser, N. Metzler-Nolte, Small organometallic compounds as antibacterial agents, Dalton Trans., 41 (2012) 6350-6358.
[19] Ł. Szczupak, A. Kowalczyk, D. Trzybiński, K. Woźniak, G. Mendoza, M. Arruebo, D. Steverding, P. Stączek, K. Kowalski, Organometallic ciprofloxacin conjugates with dual action: synthesis, characterization, and antimicrobial and cytotoxicity studies, Dalton Trans., 49 (2020) 1403-1415.
[20] K.D. Mjos, C. Orvig, Metallodrugs in Medicinal Inorganic Chemistry, Chem. Rev., 114 (2014) 4540-4563.
[21] A. Frei, A.D. Verderosa, A.G. Elliott, J. Zuegg, M.A.T. Blaskovich, Metals to combat antimicrobial resistance, Nature Reviews Chemistry, 7 (2023) 202-224.
[22] J. Delasoie, A. Pavic, N. Voutier, S. Vojnovic, A. Crochet, J. Nikodinovic-Runic, F. Zobi, Identification of novel potent and non-toxic anticancer, anti-angiogenic and antimetastatic rhenium complexes against colorectal carcinoma, Eur. J. Med. Chem., 204 (2020) 112583.
[23] E.B. Bauer, A.A. Haase, R.M. Reich, D.C. Crans, F.E. Kühn, Organometallic and coordination rhenium compounds and their potential in cancer therapy, Coord. Chem. Rev., 393 (2019) 79-117.
[24] C.C. Konkankit, S.C. Marker, K.M. Knopf, J.J. Wilson, Anticancer activity of complexes of the third row transition metals, rhenium, osmium, and iridium, Dalton Trans., 47 (2018) 9934-9974.

[25] H.S. Liew, C.-W. Mai, M. Zulkefeli, T. Madheswaran, L.V. Kiew, N. Delsuc, M.L. Low, Recent Emergence of Rhenium(I) Tricarbonyl Complexes as Photosensitisers for Cancer Therapy, Molecules, 25 (2020) 4176.
[26] K. Schindler, F. Zobi, Anticancer and Antibiotic Rhenium Tri- and Dicarbonyl Complexes: Current Research and Future Perspectives, Molecules, 27 (2022).
[27] A. Noor, G.S. Huff, S.V. Kumar, J.E.M. Lewis, B.M. Paterson, C. Schieber, P.S. Donnelly, H.J.L. Brooks, K.C. Gordon, S.C. Moratti, J.D. Crowley, [Re(CO)3]+ Complexes of exo-Functionalized Tridentate "Click" Macrocycles: Synthesis, Stability, Photophysical Properties, Bioconjugation, and Antibacterial Activity, Organometallics, 33 (2014) 7031-7043.
[28] S. Vellas, W. Lo, H. Brooks, L. Hanton, J. Crowley, Antimicrobial Properties of Mono- and Di-fac-rhenium Tricarbonyl 2-Pyridyl-1,2,3-triazole Complexes, Aust. J. Chem., 69 (2015).
[29] D. Siegmund, N. Lorenz, Y. Gothe, C. Spies, B. Geissler, P. Prochnow, P. Nuernberger, J.E. Bandow, N. Metzler-Nolte, Benzannulated Re(i)–NHC complexes: synthesis, photophysical properties and antimicrobial activity, Dalton Trans., 46 (2017) 15269-15279.
[30] A. Frei, M. Amado, M.A. Cooper, M.A.T. Blaskovich, Light-Activated Rhenium Complexes with Dual Mode of Action against Bacteria, Chem. Eur. J., 26 (2020) 2852-2858.
[31] Y. Cortat, M. Nedyalkova, K. Schindler, P. Kadakia, G. Demirci, S. Nasiri Sovari, A. Crochet, S. Salentinig, M. Lattuada, O.M. Steiner, F. Zobi, Computer-Aided Drug Design and Synthesis of Rhenium Clotrimazole Antimicrobial Agents, Antibiotics, 12 (2023) 619.
[32] K. Schindler, Y. Cortat, M. Nedyalkova, A. Crochet, M. Lattuada, A. Pavic, F. Zobi, Antimicrobial Activity of Rhenium Di- and Tricarbonyl Diimine Complexes: Insights on Membrane-Bound S. aureus Protein Binding, Pharm., 15 (2022) 1107.
[33] S.N. Sovari, T.M. Golding, M. Mbaba, R. Mohunlal, T.J. Egan, G.S. Smith, F. Zobi, Rhenium(I) derivatives of aminoquinoline and imidazolopiperidine-based ligands: Synthesis, in vitro and in silico biological evaluation against Plasmodium falciparum, J. Inorg. Biochem., 234 (2022) 111905.
[34] S.N. Sovari, N. Radakovic, P. Roch, A. Crochet, A. Pavic, F. Zobi, Combatting AMR: A molecular approach to the discovery of potent and non-toxic rhenium complexes active against C. albicans-MRSA co-infection, Eur. J. Med. Chem., 226 (2021) 113858.
[35] S.S. Mendes, J. Marques, E. Mesterházy, J. Straetener, M. Arts, T. Pissarro, J. Reginold, A. Berscheid, J. Bornikoel, R.M. Kluj, C. Mayer, F. Oesterhelt, S. Friães, B. Royo, T. Schneider, H. Brötz-Oesterhelt, C.C. Romão, L.M. Saraiva, Synergetic Antimicrobial Activity and Mechanism of Clotrimazole-Linked CO-Releasing Molecules, ACS Bio. & Med. Chem. Au, 2 (2022) 419-436.
[36] M. Wenzel, M. Patra, C.H. Senges, I. Ott, J.J. Stepanek, A. Pinto, P. Prochnow, C. Vuong, S. Langklotz, N. Metzler-Nolte, J.E. Bandow, Analysis of the mechanism of action of potent antibacterial hetero-tri-organometallic compounds: a structurally new class of antibiotics, ACS Chem. Biol., 8 (2013) 1442-1450.
[37] M. Patra, M. Wenzel, P. Prochnow, V. Pierroz, G. Gasser, J.E. Bandow, N. Metzler-Nolte, An organometallic structure-activity relationship study reveals the essential role of a Re(CO)3 moiety in the activity against gram-positive pathogens including MRSA, Chem. Sci. J., 6 (2015) 214-224.
[38] S.N. Sovari, S. Vojnovic, S.S. Bogojevic, A. Crochet, A. Pavic, J. Nikodinovic-Runic, F. Zobi, Design, synthesis and in vivo evaluation of 3-arylcoumarin derivatives of rhenium(I) tricarbonyl complexes as potent antibacterial agents against methicillin-resistant Staphylococcus aureus (MRSA), Eur. J. Med. Chem., 205 (2020) 112533.
[39] A. Jashari, F. Imeri, L. Ballazhi, A. Shabani, B. Mikhova, G. Dräger, E. Popovski, A. Huwiler, Synthesis and cellular characterization of novel isoxazolo- and thiazolohydrazinylidene-chroman-2,4-diones on cancer and non-cancer cell growth and death, Bioorg. Med. Chem., 22 (2014) 2655-2661.
[40] F. Rahmani, A. Crochet, F. Zobi, (E)-3-(2-(4-methylthiazol-2-yl)hydrazineylidene)chromane-2,4-dione, Molbank., 2022 (2022) M1504.
[41] M. B, Y.D. Bodke, N. O, L.T. N, N. G, S. Ma, Coumarin-Benzothiazole Based Azo Dyes: Synthesis, Characterization, Computational, Photophysical and Biological Studies, J. Mol. Struct., 1246 (2021) 131170.

[42] J.K. Adu, C.D.K. Amengor, N. Mohammed Ibrahim, C. Amaning-Danquah, C. Owusu Ansah, D.D. Gbadago, J. Sarpong-Agyapong, Synthesis and In Vitro Antimicrobial and Anthelminthic Evaluation of Naphtholic and Phenolic Azo Dyes, J. Trop. Med., 2020 (2020) 4850492.
[43] A. Geronikaki, P. Vicini, N. Dabarakis, A. Lagunin, V. Poroikov, J. Dearden, H. Modarresi, M. Hewitt, G. Theophilidis, Evaluation of the local anaesthetic activity of 3-aminobenzo[d]isothiazole derivatives using the rat sciatic nerve model, Eur. J. Med. Chem., 44 (2009) 473-481.
[44] C. Papadopoulou, A. Geronikaki, D. Hadjipavlou-Litina, Synthesis and biological evaluation of new thiazolyl/benzothiazolyl-amides, derivatives of 4-phenyl-piperazine, Il Farmaco, 60 (2005) 969-973.
[45] M.A. Gouda, M.A. Berghot, E.A. Baz, W.S. Hamama, Synthesis, antitumor and antioxidant evaluation of some new thiazole and thiophene derivatives incorporated coumarin moiety, Med. Chem. Res 21 (2012) 1062-1070.
[46] M.D. Naik, Y.D. Bodke, V.K. M, R. Bc, An efficient one-pot synthesis of coumarin-amino acid derivatives as potential anti-inflammatory and antioxidant agents, Synth. Commun. , 50 (2020) 1210-1216.
[47] R.S. Keri, S. B.S, B.M. Nagaraja, M.A. Santos, Recent progress in the drug development of coumarin derivatives as potent antituberculosis agents, Eur. J. Med. Chem., 100 (2015) 257-269.
[48] C.A. Kontogiorgis, D.J. Hadjipavlou-Litina, Synthesis and Antiinflammatory Activity of Coumarin Derivatives, J. Med. Chem., 48 (2005) 6400-6408.
[49] B.S. Kirkiacharian, E. De Clercq, R. Kurkjian, C. Pannecouque, New synthesis and anti-HIV and antiviral properties of 3-arylsulfonyl derivatives of 4-ydroxycoumarin and 4-hydroxyquinolone, Pharm. Chem. J., 42 (2008) 265-270.
[50] P.K. Jauhari, A. Bhavani, S. Varalwar, K. Singhal, P. Raj, Synthesis of some novel 2-substituted benzoxazoles as anticancer, antifungal, and antimicrobial agents, Med. Chem. Res, 17 (2008) 412-424.
[51] B. Soni, M.S. Ranawat, R. Sharma, A. Bhandari, S. Sharma, Synthesis and evaluation of some new benzothiazole derivatives as potential antimicrobial agents, Eur. J. Med. Chem., 45 (2010) 2938-2942.
[52] S.P. Schmidt, W.C. Trogler, F. Basolo, M.A. Urbancic, J.R. Shapley, Pentacarbonylrhenium Halides, in: Inorg. Synth., 1990, pp. 160-165.
[53] P. Kurz, B. Probst, B. Spingler, R. Alberto, Ligand Variations in [ReX(diimine)(CO)3] Complexes: Effects on Photocatalytic CO2 Reduction, Eur. J. Inorg. Chem., 2006 (2006) 2966-2974.
[54] B. Stamboliyska, A. Jashari, D. Yancheva, B. Mikhova, D. Batovska, E. Popovski, K. Mladenovska, Structure and radical scavenging activity of isoxazolo-and thiazolohydrazinylidene-chromaffin-2, 4-diones, Bulg. Chem. Commun., (2017).
[55] Y.-P. Hsu, E. Hall, G. Booher, B. Murphy, A.D. Radkov, J. Yablonowski, C. Mulcahey, L. Alvarez, F. Cava, Y.V. Brun, E. Kuru, M.S. VanNieuwenhze, Fluorogenic d-amino acids enable real-time monitoring of peptidoglycan biosynthesis and high-throughput transpeptidation assays, Nat. Chem., 11 (2019) 335-341.
[56] E. Kuru, S. Tekkam, E. Hall, Y.V. Brun, M.S. Van Nieuwenhze, Synthesis of fluorescent D-amino acids and their use for probing peptidoglycan synthesis and bacterial growth in situ, Nat. Protoc., 10 (2015) 33-52.
[57] E. Kuru, A. Radkov, X. Meng, A. Egan, L. Alvarez, A. Dowson, G. Booher, E. Breukink, D.I. Roper, F. Cava, W. Vollmer, Y. Brun, M.S. VanNieuwenhze, Mechanisms of Incorporation for D-Amino Acid Probes That Target Peptidoglycan Biosynthesis, ACS Chem. Biol., 14 (2019) 2745-2756.
[58] N.M. Brown, A.L. Goodman, C. Horner, A. Jenkins, E.M. Brown, Treatment of methicillin-resistant Staphylococcus aureus (MRSA): updated guidelines from the UK, JAC-AMR, 3 (2021).
[59] F. Gudiol, J.M. Aguado, B. Almirante, E. Bouza, E. Cercenado, M.Á. Domínguez, O. Gasch, J. Lora-Tamayo, J.M. Miró, M. Palomar, A. Pascual, J.M. Pericas, M. Pujol, J. Rodríguez-Baño, E. Shaw, A. Soriano, J. Vallés, Diagnosis and treatment of bacteremia and endocarditis due to Staphylococcus aureus. A clinical guideline from the Spanish Society of Clinical Microbiology and Infectious Diseases (SEIMC), Enferm. Infecc. Microbiol. Clin., 33 (2015) 625.e621-625.e623.

[60] Y.-S. Chen, Guidelines for the treatment of methicillin-resistant Staphylococcus aureus infections in Taiwan, J. Microbiol. Immunol. Infect., 46 (2013) 147-150.
[61] C. Liu, A. Bayer, S.E. Cosgrove, R.S. Daum, S.K. Fridkin, R.J. Gorwitz, S.L. Kaplan, A.W. Karchmer, D.P. Levine, B.E. Murray, M.J. Rybak, D.A. Talan, H.F. Chambers, Clinical Practice Guidelines by the Infectious Diseases Society of America for the Treatment of Methicillin-Resistant Staphylococcus aureus Infections in Adults and Children, Clin. Infect. Dis., 52 (2011) e18-e55.
[62] A.L. Lovering, L.H. de Castro, D. Lim, N.C.J. Strynadka, Structural Insight into the Transglycosylation Step of Bacterial Cell-Wall Biosynthesis, Science, 315 (2007) 1402-1405.
[63] A.L. Lovering, M.C. Gretes, S.S. Safadi, F. Danel, L. de Castro, M.G.P. Page, N.C.J. Strynadka, Structural Insights into the Anti-methicillin-resistant Staphylococcus aureus (MRSA) Activity of Ceftobiprole*, J. Biol. Chem., 287 (2012) 32096-32102.
[64] H. Yoshida, F. Kawai, E. Obayashi, S. Akashi, D.I. Roper, J.R.H. Tame, S.-Y. Park, Crystal Structures of Penicillin-Binding Protein 3 (PBP3) from Methicillin-Resistant Staphylococcus aureus in the Apo and Cefotaxime-Bound Forms, J. Mol. Biol., 423 (2012) 351-364.
[65] J.A.N. Alexander, S.S. Chatterjee, S.M. Hamilton, L.D. Eltis, H.F. Chambers, N.C.J. Strynadka, Structural and kinetic analyses of penicillin-binding protein 4 (PBP4)-mediated antibiotic resistance in Staphylococcus aureus, J. Biol. Chem., 293 (2018) 19854-19865.
[66] L. Boulos, M. Prévost, B. Barbeau, J. Coallier, R. Desjardins, LIVE/DEAD® BacLight™: application of a new rapid staining method for direct enumeration of viable and total bacteria in drinking water, J. Microbiol. Methods, 37 (1999) 77-86.
[67] E. Kuru, S. Tekkam, E. Hall, Y.V. Brun, M.S. Van Nieuwenhze, Synthesis of fluorescent D-amino acids and their use for probing peptidoglycan synthesis and bacterial growth in situ, Nature Protocols, 10 (2015) 33-52.
[68] F. Nallet, R. Laversanne, D. Roux, Modelling X-ray or neutron scattering spectra of lyotropic lamellar phases : interplay between form and structure factors, J. Phys. II France, 3 (1993) 487-502.
[69] R.V.M. Freire, Y. Pillco-Valencia, G.C.A. da Hora, M. Ramstedt, L. Sandblad, T.A. Soares, S. Salentinig, Antimicrobial peptide induced colloidal transformations in bacteria-mimetic vesicles: Combining in silico tools and experimental methods, J. Colloid Interface Sci., 596 (2021) 352-363.
[70] P. Bellio, L. Fagnani, L. Nazzicone, G. Celenza, New and simplified method for drug combination studies by checkerboard assay, MethodsX, 8 (2021) 101543.
[71] J.-D. Chai, M. Head-Gordon, Systematic optimization of long-range corrected hybrid density functionals, J. Chem. Phys., 128 (2008).
[72] J.-D. Chai, M. Head-Gordon, Long-range corrected hybrid density functionals with damped atom–atom dispersion corrections, PCCP, 10 (2008) 6615-6620.
[73] A.D. Becke, Density-functional thermochemistry. V. Systematic optimization of exchange-correlation functionals, J. Chem. Phys., 107 (1997) 8554-8560.
[74] Q. Wu, W. Yang, Empirical correction to density functional theory for van der Waals interactions, J. Chem. Phys., 116 (2002) 515-524.
[75] D. Andrae, U. Häußermann, M. Dolg, H. Stoll, H. Preuß, Energy-adjustedab initio pseudopotentials for the second and third row transition elements, Theor. Chim. Acta, 77 (1990) 123-141.
[76] M.M. Jaghoori, B. Bleijlevens, S.D. Olabarriaga, 1001 Ways to run AutoDock Vina for virtual screening, J. Comput. Aided Mol. Des., 30 (2016) 237-249.
[77] R. Agarwal, J.C. Smith, Speed vs Accuracy: Effect on Ligand Pose Accuracy of Varying Box Size and Exhaustiveness in AutoDock Vina, Mol. Inform., 42 (2023) 2200188.
[78] X. Che, Q. Liu, L. Zhang, An accurate and universal protein-small molecule batch docking solution using Autodock Vina, RINENG, 19 (2023) 101335.